Molecular Therapy
Original Article

Gene Therapeutic Reversal of Peripheral Olfactory Impairment in Bardet-Biedl Syndrome

Corey L. Williams,[1,2,5] Cedric R. Uytingco,[1,2,5] Warren W. Green,[1,2] Jeremy C. McIntyre,[1,2] Kirill Ukhanov,[1,2] Arthur D. Zimmerman,[1,2] Dana T. Shively,[1,2] Lian Zhang,[1,2] Darryl Y. Nishimura,[3] Val C. Sheffield,[3,4] and Jeffrey R. Martens[1,2]

[1]Department of Pharmacology and Therapeutics, University of Florida College of Medicine, Gainesville, FL 32610, USA; [2]Center for Smell and Taste, University of Florida College of Medicine, Gainesville, FL 32610, USA; [3]Department of Pediatrics, University of Iowa, Iowa City, IA 52242, USA; [4]Howard Hughes Medical Institute, University of Iowa, Iowa City, IA 52242, USA

Olfactory dysfunction is a pervasive but underappreciated health concern that affects personal safety and quality of life. Patients with olfactory dysfunctions have limited therapeutic options, particularly those involving congenital diseases. Bardet-Biedl syndrome (BBS) is one such disorder, where olfactory loss and other symptoms manifest from defective cilium morphology and/or function in various cell types/tissues. Olfactory sensory neurons (OSNs) of BBS mutant mice lack the capacity to build/maintain cilia, rendering the cells incapable of odor detection. Here we examined OSN cilium defects in *Bbs1* mutant mice and assessed the utility of gene therapy to restore ciliation and function in young and adult mice. *Bbs1* mutant mice possessed short residual OSN cilia in which BBSome protein trafficking and odorant detection were defective. Gene therapy with an adenovirus-delivered wild-type *Bbs1* gene restored OSN ciliation, corrected BBSome cilium trafficking defects, and returned acute odor responses. Finally, using clinically approved AAV serotypes, we demonstrate, for the first time, the capacity of AAVs to restore ciliation and odor detection in OSNs of Bbs1 mutants. Together, our data demonstrate that OSN ciliogenesis can be promoted in differentiated cells of young and adult *Bbs1* mutants and highlight the potential of gene therapy as a viable restorative treatment for congenital olfactory disorders.

INTRODUCTION

Human ciliopathies are a growing class of hereditary disorders in which altered cilium formation and/or function underlie pathogenesis. Ciliopathies encompass syndromes that affect single organs as well as highly pleiotropic diseases that exhibit systemic penetrance. Phenotypes include bone anomalies, situs inversus, heart malformation, neurological defects, ataxia, infertility, renal dysplasia, and sensory deficits.[1] Bardet-Biedl syndrome (BBS) (Online Mendelian Inheritance in Man #209900) is an autosomal recessive and broadly pleiotropic ciliopathy that features postaxial polydactyly followed by the onset of obesity, retinal degeneration, and renal failure.[2,3] In addition, BBS patients have variably penetrant olfactory deficits that range from mild microsmia to full anosmia.[4,5]

BBS is a genetically heterogeneous disease with 21 identified loci to date (http://www.ncbi.nlm.nih.gov/pubmed/27008867). Eight BBS gene products interact together in a core complex known as the BBSome.[6] The BBSome is postulated to function as a membrane coat complex that drives ciliary membrane biogenesis and regulates the ciliary trafficking of polytopic membrane proteins through an interaction with intraflagellar transport (IFT) machinery.[7–12] IFT is an evolutionarily conserved protein trafficking system that mediates anterograde and retrograde movement along ciliary microtubule axonemes and is essential for cilium formation and maintenance.[13] We and others have demonstrated that components of the BBSome participate in IFT in mammals and lower eukaryotes;[12–17] however, the exact functional role of the BBSome in the mammalian IFT is unclear. Importantly, loss of BBSome function in murine BBS models typically alters ciliary signaling capabilities and polytopic membrane protein localization in different cell types with diverse effects on cilium biogenesis. Therefore, the penetrance of BBS phenotypes in different organ systems is variable. The olfactory epithelium (OE) is one location where ciliation is dramatically decreased.[4,18–20] accounting for anosmia observed in BBS patients. This body of evidence, across several tissues and organisms, suggests that the precise role of the BBSome in normal ciliary trafficking and/or function varies by cell type, which may underlie the pleotropic nature of BBS.

Although clinical treatments for BBS and other ciliopathy patients are limited, our expanding comprehension of ciliopathy genetics enables the pursuit of gene therapy as a curative measure. It is estimated that roughly 80% of all BBS cases can be attributed to one of the known disease loci,[21] indicating that personalized medicine is a viable option for most patients. Previously, we demonstrated that ectopic gene introduction via intranasal viral delivery is an effective measure to

Received 18 November 2016; accepted 5 February 2017;
http://dx.doi.org/10.1016/j.ymthe.2017.02.006.

[5]These authors contributed equally to this work.

Correspondence: Jeffery R. Martens, Department of Pharmacology and Therapeutics, University of Florida, 1200 Newell Drive, PO Box 100267, Gainesville, FL 32610-0267, USA.
E-mail: martensj@ufl.edu

restore olfactory cilium function and enable sensory detection in a hypomorphic mouse model of a severe prenatal lethal ciliopathy.[22] Here we tested the potential of gene therapy to restore odor detection in a BBS1 murine disease model that represents one of the three most commonly mutated BBS genes.[2,23] We report that noninvasive intranasal delivery of the wild-type (WT) BBS1 gene via adenovirus serotype 5 (AV5) is sufficient to restore ciliation of olfactory sensory neurons (OSNs), correct ciliary trafficking defects, and improve odor detection in both young and adult BBS mutant animals. Importantly, we demonstrate that clinically relevant adeno-associated virus serotype 9 (AAV9) is also effective for transduction of the OE and restoration of ciliation and odor detection in mutant animals. Our data indicate that BBS gene therapy can initiate ciliogenesis in differentiated mutant cells in vivo and that it represents a viable approach for treating olfactory deficits in BBS patients.

RESULTS

Reduced OSN Cilium Length and Number in BBS Mutant Mice

Olfactory deficits have been described in several BBS mouse models.[4,18,20,24–26] To examine gene therapy as a potential treatment option in BBS-associated anosmia and limit the effect of exogenous tissues, we used an OSN-specific knockout of *Bbs1* (*Bbs1*^{osnKO}). This strain was generated by combining a floxed *Bbs1* allele[27] with an *OMP-Cre* allele[28] that expresses Cre recombinase specifically in mature OSNs. Homozygous floxed *Bbs1* mice carrying a single *OMP-Cre* allele were used as mutants throughout this study; control animals carried at least one WT *Bbs1* allele or lacked the *OMP-Cre* allele. We first assessed the status of OSN cilia in the OE of *Bbs1*^{osnKO} animals. The OE is a pseudo-stratified epithelium in which the OSN dendrites extend apically toward the nasal cavity lumen, forming knobs decorated with cilia. These cilia form a meshwork on the OE surface that can be visualized by immunostaining of acetylated α-tubulin, a marker of ciliary microtubules. Compared with control mice, *Bbs1*^{osnKO} mutants showed global acetylated α-tubulin signal reduction on the OE apical surface (highlighted via OMP immunoreactivity), suggesting a loss of OSN cilia (Figures 1A, 1B, 1D, and 1E). Similar to reports on other BBS models,[4,20] *Bbs1*^{osnKO} mutants did not show acetylated α-tubulin reduction on the apical surface of the respiratory epithelium (where OMP is not expressed) (Figures 1D and 1E). The reduction in acetylated α-tubulin immunostaining is concomitant with diminished endogenous ACIII (Figures S1A–S1C) and cyclic nucleotide gated channel alpha 2 (Cnga2) immunostaining in *Bbs1*^{osnKO} mutants (Figures S1D–S1F).[4,18] To confirm that decreased acetylated α-tubulin, adenylate cyclase III (ACIII), and CNGA2 signals corresponded to OSN cilium loss, we performed scanning electron microscopy on the olfactory turbinates of *Bbs1*^{osnKO} animals and found diminished ciliation (Figures 1C and 1F). Notably, OSNs possessed residual cilia among the exposed microvilli of the underlying supporting cells (Figure 1F). To examine the composition and morphology of the residual OSN cilia of BBS mutants, we next employed adenovirus (AV)-mediated ectopic expression of fluorescent protein-tagged cilium markers and live en face confocal imaging of the OE surface (Figures 1G and 1H). Compared with examination of coronal cryosections of fixed tissues, live en face confocal imaging allows for detailed examination of intact cilia, cilium structure, and protein trafficking dynamics limiting the contribution of artifacts,[14] Combined with AV5-mediated expression of the myristoylated-palmitoylated form of mCherry (MyrPalm-mCherry), an inert probe that marks the cell and ciliary membrane inner leaflet, we are able to visualize and confirm the full length of OSN cilia.[14] We next assessed the localization of polytopic membrane proteins that are part of the olfactory signaling pathway and enriched in the cilia. Ectopic co-expression of GFP-fused adenylate cyclase III (ACIII-GFP) and MyrPalm-mCherry showed ACIII-GFP presence in residual OSN cilia of *Bbs1*^{osnKO} animals (Figure S2A), suggesting that BBS1 was not essential for ACIII entry into OSN cilia. This is consistent with previous reports[4,18] and diminished endogenous ACIII and Cnga2 immunostaining in *Bbs1*^{osnKO} mutant coronal sections (Figure S1). Using AV5-mediated expression of MyrPalm-mCherry, we next examined the degree of OSN ciliation across the turbinates of the OE. Analysis of cilia from control animals showed uniform OSN cilium lengths and numbers across the turbinate surface of the OE (Figure S3), which are consistent with past reports.[29–32] We next quantified the extent of OSN cilium loss in *Bbs1*^{osnKO} animals. Compared with controls, *Bbs1*^{osnKO} animals had significantly reduced cilium length, resulting in a leftward shift in the cumulative distribution of total cilia (Figure 1J; Figure S3). In *Bbs1*^{osnKO} mutants, OSN cilium length was reduced by 77% (6.11 ± 0.15 μm) from control (26.61 ± 0.63 μm), whereas the cilium number per OSN was reduced by half in *Bbs1*^{osnKO} mutants (12.22 ± 0.49 cilia) from the control (23.07 ± 0.95 cilia) (Figures 1K and 1L; Figure S3). Overall, our results indicate that *Bbs1*^{osnKO} mutants retain the capacity to build OSN cilia but are unable to attain or maintain normal OSN cilium length or number.

Impaired BBSome Trafficking in *Bbs1*^{osnKO} Mutant Mice

Our findings of shorter and fewer OSN cilia in *Bbs1*^{osnKO} mutants prompted us to analyze cilium protein trafficking in the animals. Previous work has uncovered specific interactions between BBS proteins[33] and their assembly into the BBSome;[34] however, BBS protein function in mammalian protein trafficking in the cilia and BBSome ciliary targeting are unclear. We therefore examined the effect of BBS1 disruption on the ciliary localization and IFT of other BBSome proteins. Using total internal reflection fluorescence (TIRF) microscopy, which allows visualization of cilium protein trafficking,[14] we examined IFT within the residual cilia. Interestingly, we found that IFT was retained in *Bbs1*^{osnKO} mutant OSN cilia (Figures 2A, 2B, and 2E). Components of the heterotrimeric kinesin II (Kap3a) and cytoplasmic dynein motor (Dync2li1) complexes, which associate with the IFT particles, showed cilium trafficking and bidirectional transport in *Bbs1*^{osnKO} mutants (Figures 2A and 2B; Figure S2B). Next we assessed the cilium trafficking of BBSome proteins. We demonstrated that BBS1, BBS2, BBS4, and BBS5 undergo IFT in OSN cilia.[14] In *BBS1*^{osnKO} mutants, ectopically expressed BBS2-GFP, BBS4-GFP, and BBS5-GFP fail to localize within the cilia despite heavily accumulating in OSN dendritic knobs (Figures 2C and 2D). To confirm this result, we co-expressed BBS4-mCherry and Kap3a-GFP in *Bbs1*^{osnKO} mutants and did not find co-localization

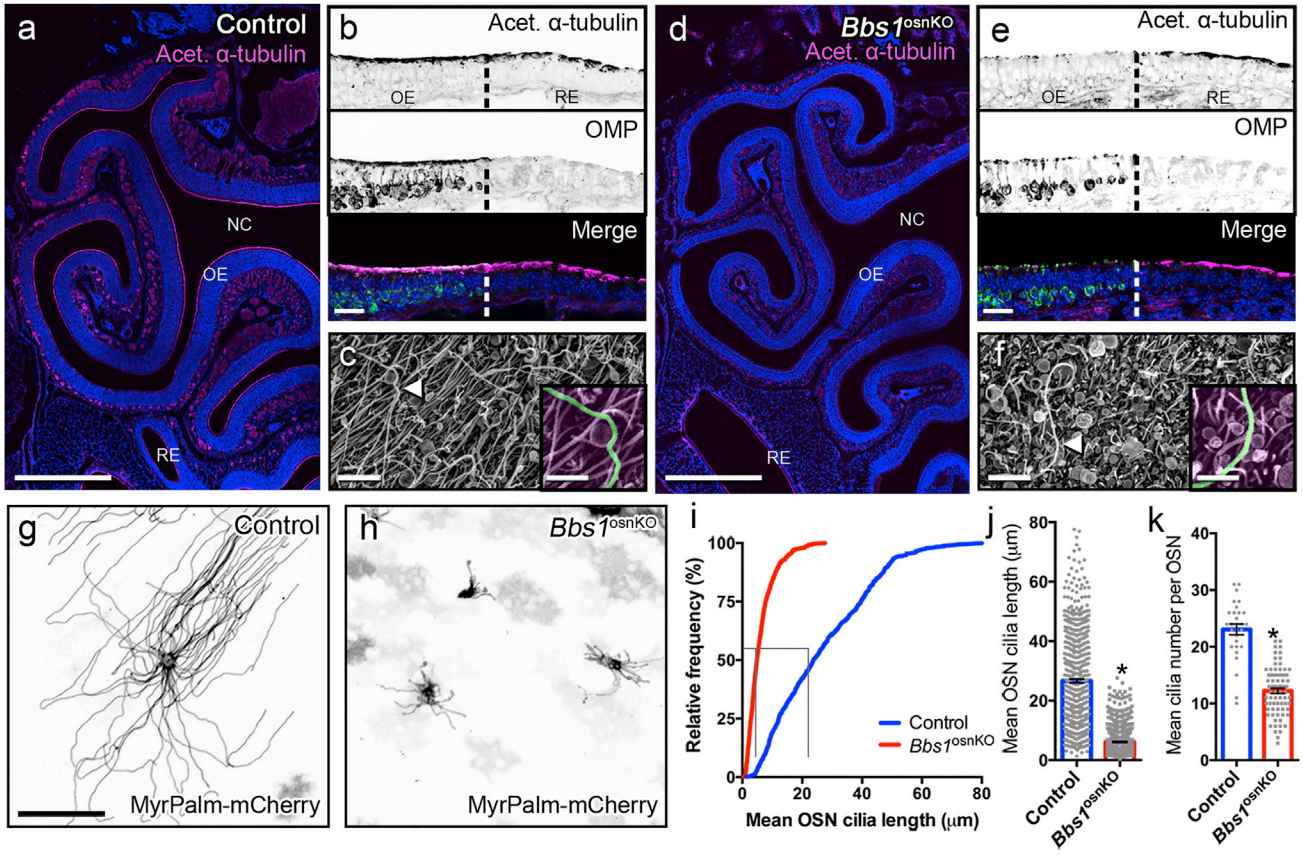

Figure 1. Olfactory Cilium Loss in *Bbs1*^{osnKO} Mutant Mice

(A and D) Representative global confocal images of coronal sections through nasal epithelium of (A) control and (D) *Bbs1*^{osnKO} mutant mice, immunostained for acetylated α-tubulin to reveal ciliary microtubules. The OE and respiratory epithelium (RE) line the turbinates of the nasal cavity (NC). (B and E) Representative olfactory and respiratory epithelia of (B) control and (E) *Bbs1*^{osnKO} mutant mice, immunostained for (top) acetylated α-tubulin to reveal ciliary microtubules and (center) olfactory marker protein (OMP) to reveal mature OSNs. Dashed lines demarcate the OE and RE boundary. Compared (A and B) the control, (D and E) *Bbs1*^{osnKO} have reduced acetylated α-tubulin in the OE. (C and F) Representative scanning electron micrographs of the OE surface in control and mutant mice. Compared with (C) control tissue, (F) *Bbs1*^{osnKO} tissues possess very few cilia (arrowheads, magnified insets), exposing the underlying sustentacular microvilli. (G and H) Representative live en face confocal images of ectopically expressed MyrPalm-mCherry in OSN cilia of control and mutant mice. Compared with (G) the control, (H) *Bbs1*^{osnKO} OSNs possess fewer and shorter cilia. (I) Cumulative distribution of cilium lengths from (blue) control and (red) *Bbs1*^{osnKO} en face confocal images. (J and K) Quantification of reduced mean (J) OSN cilium length and (K) cilium number in *Bbs1*^{osnKO} mutants, measured from live en face confocal images of ectopically expressed MyrPalm-mCherry (control n = 669 cilia on 29 OSNs; *Bbs1*^{osnKO} n = 895 cilia on 74 OSNs). Student's t test, *p < 0.0001. Values represent means ± SEM. Scale bars, 500 μm (A and D), 20 μm (B and E), 2.5 μm (C and F), 1.25 μm (C and F, insets), and 20 μm (G and H).

of BBS4-mCherry on IFT particles in residual cilia (Figure 2E). Although not required for the assembly of the BBSome complex[34] and IFT, these data suggest that BBS1 is essential for BBSome entry into the cilia.

Odor Detection and Glomerular Morphology Defects in *Bbs1*^{osnKO} Mutant Mice

To measure the effect of OSN cilium loss on odor detection in *Bbs1*^{osnKO} mutants, we performed electro-olfactogram (EOG) recordings, which measure the changes in summated field potential generation from OSN populations in response to odorant exposure. Compared with controls, *Bbs1*^{osnKO} mutants showed reduced electrical responses in a concentration-dependent manner to amyl acetate as well as to a single non-saturating concentration of several odors (Figures 3A–3C). These results support the notion that defective OSN ciliation in *Bbs1*^{osnKO} mutants translates to olfactory dysfunction on the level of odor detection. Normally, odor-driven stimulation of OSN synaptic activity induces expression of tyrosine hydroxylase (TH) in dopaminergic juxtaglomerular interneurons that innervate glomeruli of the olfactory bulb.[35] Consistent with impaired odor detection, we measured reduced TH expression in the olfactory bulbs of *Bbs1*^{osnKO} mutants (Figure 3D). *Bbs1*^{osnKO} mutants also exhibited a reduction in glomerular size (Figure 3E), which likely corresponds to OSN axon pathfinding defects from the loss of olfactory signaling[36–38] and is consistent in other BBS mouse models[18] as well as naris occlusion models.[38,39] Together, the loss of odorant detection and reduction

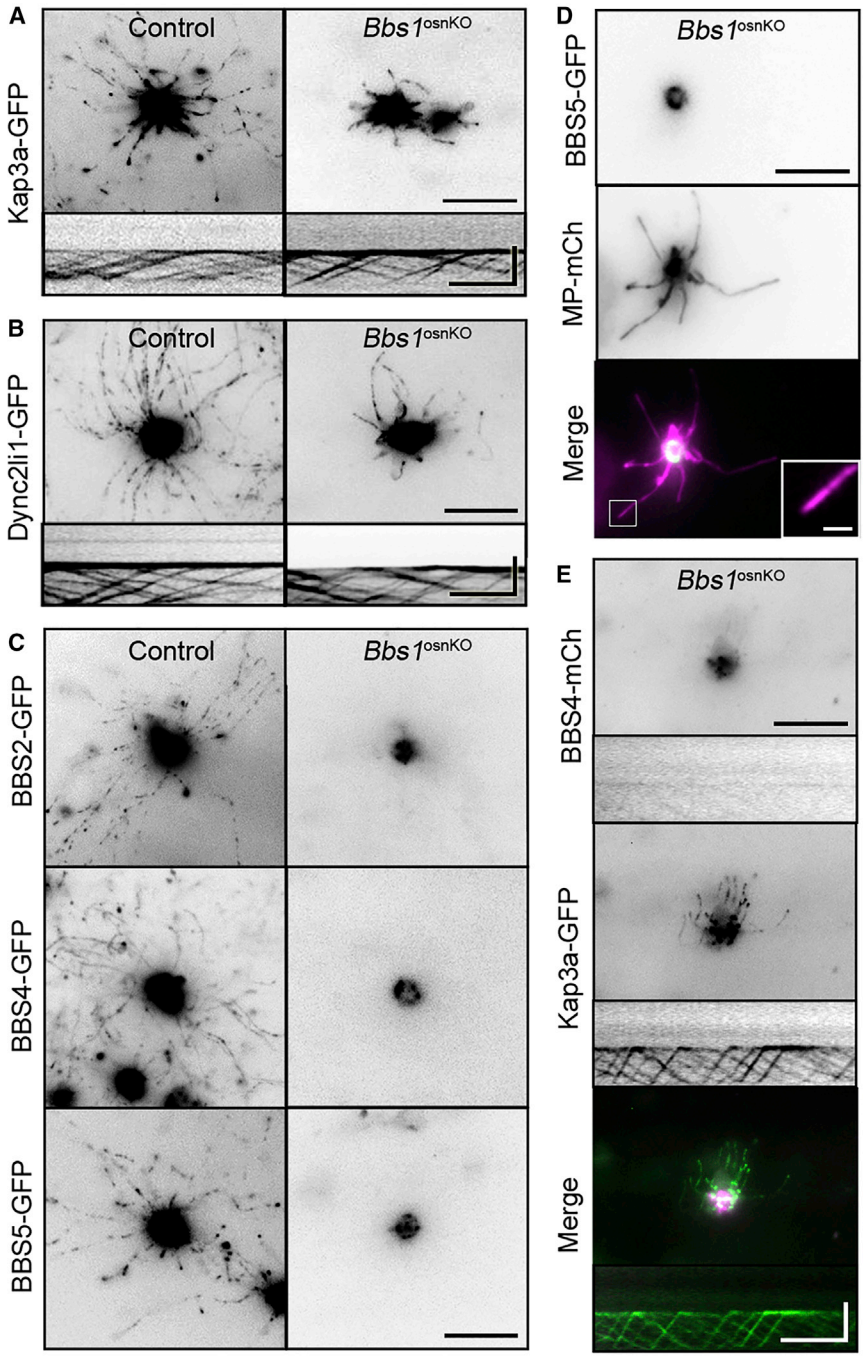

Figure 2. Role of BBS1 in IFT and BBSome Trafficking

(A) Representative en face TIRF microscopy images of ectopically expressing tagged heterotrimeric kinesin II (Kap3a-GFP) in (left) control and (right) *Bbs1*^{osnKO} OSN cilia. Bottom: representative kymograms showing Kap3a-GFP trafficking. (B) En face TIRF microscopy images of ectopically expressing tagged dynein motor (Dync2li1-GFP) in (left) control and (right) *Bbs1*^{osnKO} OSN cilia. Bottom: representative kymograms showing Dync2li1-GFP trafficking. (C) Representative en face TIRF microscopy images of ectopically expressing tagged BBS proteins ectopically expressed in control and mutant OSNs. In (left) the control, BBSome subunits are expressed in OSN dendritic knobs and cilia. In (right) *Bbs1*^{osnKO} OSNs, BBSome subunits are restricted to knobs. (D) Representative en face TIRF microscopy images of OSNs co-expressing BBS5-GFP and MyrPalm-mCherry (MP-mCh). BBS5-GFP is absent in residual cilia of *Bbs1*^{osnKO} OSNs, as revealed by MyrPalm-mCherry expression. (E) En face TIRF microscopy images of a *Bbs1*^{osnKO} OSN ectopically expressing BBS4-mCherry and Kap3a-GFP. Single cilium kymograms show robust Kap3a transport (center), but BBS4-GFP (top) is absent from IFT particles. Scale bars, 10 μm, 1.25 μm (inset), and 5 μm × 30 s (kymograms in A, B, and E).

in TH immunostaining and glomerular size support the involvement of OSN ciliation for proper olfactory function.

Interestingly, we found that OSN-specific ablation of BBS1 did not result in the onset of obesity, which is a hallmark BBS phenotype in both humans and mice (Figure S4). These data suggests that olfactory dysfunction alone does not directly drive the obesity phenotype in BBS and supports previous data indicating that ciliopathy-associated obesity arises as a consequence of altered ciliary signaling in a subset of central neurons.[40]

Gene Therapy Promotes Ciliation and Enables BBSome Trafficking in *Bbs1*^{osnKO} Mutant Mice

Similar to BBS patients, *Bbs1*^{osnKO} mice have olfactory deficits, and we find that these deficits originate from loss of odor detection via diminished OSN ciliation. This loss-of-function mouse model, combined with the accessibility of the OE and the size of the *Bbs1* gene, makes *Bbs1*^{osnKO} mutant mice amenable to gene therapeutic rescue. Our previous work showed that tagged BBS proteins, including BBS1, undergo IFT in OSN cilia,[14] suggesting that these recombinant proteins retain proper function. To assess the potential of gene therapy to correct BBS olfactory phenotypes, we used AV5-mediated ectopic expression of the full-length wild-type protein BBS1-mCherry in *Bbs1*^{osnKO} mutants. Mutant animals received intranasal AV5-BBS1-mCherry doses on 3 consecutive days and were then allowed 10 days for expression. Using acetylated α-tubulin immunostaining, we examined whether ectopic expression of WT BBS genes could promote ciliation in the OE of mutant animals. In coronal OE sections from treated mutant animals, we observed global BBS1-mCherry protein expression throughout the OE (Figure 4A) and increased acetylated α-tubulin immunostaining

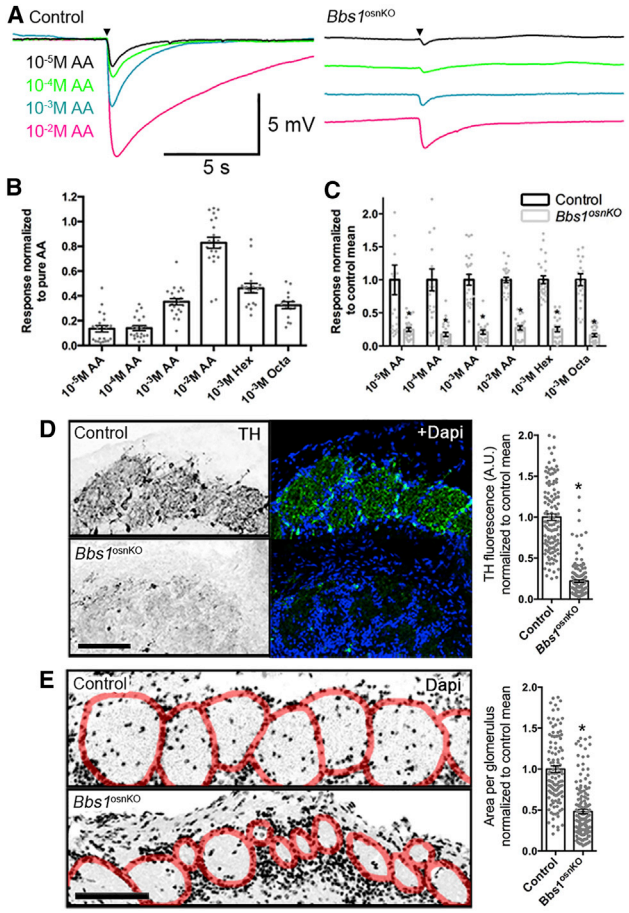

Figure 3. Odor Detection Is Reduced in *Bbs1*^{osnKO} Mutant Mice

(A) Representative EOG recordings from the OE surface of control and mutants in response to varying amyl acetate (AA) concentrations. Arrowheads indicate the time of odor delivery. (B and C) Quantified EOG data showing AA dose-dependent, hexanal (Hex), or octanol (Oct) responses in (B) the control and normalized responses in (C) *Bbs1*^{osnKO} mutants. Student's t test, *p < 0.005. (D) Representative confocal images of coronal olfactory bulb slices showing reduced glomerular TH immunoreactivity in (center) *Bbs1*^{osnKO} animals. Right: Quantification of mean TH fluorescence is reduced in *Bbs1*^{osnKO} mutants compared with the control. Student's t test, *p < 0.001. (E) Representative confocal images of DAPI-stained coronal olfactory bulb slices depicting individual glomeruli (red). Glomerular size is reduced in *Bbs1*^{osnKO} mutants compared with the control. Quantified data (right) show a nearly 50% reduction in mean glomerular size in mutant animals. Student's t test, *p < 0.0001. Values represent means ± SEM. Scale bars, 5 mV × 5 s (A) and 100 μm (D and E).

intensity in areas surrounding mCherry-positive OSN dendritic knobs (Figures 4A and 4B), suggesting that ciliation was enhanced specifically on AV5-transduced OSNs. To confirm that an increased acetylated α-tubulin signal corresponded to rescued OSN ciliation, we employed live en face confocal imaging of the OE surface of *Bbs1*^{osnKO} mutant animals that had been treated with AV5-BBS1-mCherry together with a full-length cilium marker, AV5-MyrPalm-GFP (Figure 5A). Compared with MyrPalm-GFP only expressing OSNs, cilium length and number were restored to control levels in

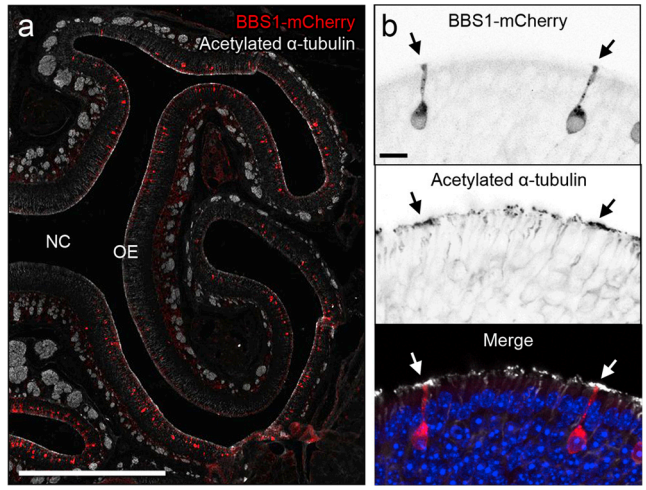

Figure 4. Global Gene Therapy-Mediated Restoration of Ciliation in *Bbs1*^{osnKO} Mutant OSNs

(A and B) Ectopic BBS1-mCherry expression in the OE. (A) Representative confocal image showing a coronal OE section from a young *Bbs1*^{osnKO} animal 10 days after intranasal AV5-BBS1-mCherry delivery. The coronal section was immunostained with acetylated α-tubulin to visualize ciliary microtubules of OSNs lining the NC. (B) Ciliary restoration surrounding AV-treated OSNs. OE coronal sections from *Bbs1*^{osnKO} animals after AV5-BBS1-mCherry treatment and immunostained for acetylated α-tubulin. The acetylated α-tubulin signal was increased near dendritic knobs (arrows) projecting from AV-transduced OSNs. Scale bars, 500 μm (A) and 10 μm (B).

OSNs co-expressing BBS1-mCherry (Figures 5A and 5B). Employing the same dosage regimen of AV5-MyrPalm-mCherry to OMP-GFP mice, we estimate an infection of 40–50 OSNs per millimeter of OE, approximately 15% of total mature OSNs.

Next we assessed the capacity of BBS gene therapy to restore BBSome ciliary localization and trafficking. *Bbs1*^{osnKO} mutant animals were intranasally treated with AV5-BBS1-mCherry together with AV5-BBS2-GFP, AV5-BBS4-GFP, or AV5-BBS5-GFP and, 10 days later, subjected to live en face TIRFm. We found that ectopic expression of BBS1-mCherry was sufficient to reestablish OSN ciliary localization of each of the BBSome proteins examined (Figures 5C–5F). By comparison, *Bbs1*^{osnKO} mutant OSNs lacking BBS1-mCherry expression remained unable to localize other BBSome proteins within residual cilia (Figure 5E). In addition, bidirectional particle trafficking of BBSome proteins was restored in cilia on mutant OSNs expressing BBS1-mCherry (Figures 5G–5J). Together, these data show that, in addition to promoting ciliation in BBS mutant OSNs, gene therapy also rescues BBSome cilium localization and ciliary protein trafficking defects.

Gene Therapy Restores Odor Detection in *Bbs1*^{osnKO} Mutant Mice

Based on our rescue of OSN ciliation and BBSome ciliary trafficking in BBS mutants, we hypothesized that odor detection would also be restored in treated animals. Young *Bbs1*^{osnKO} mutants were intranasally

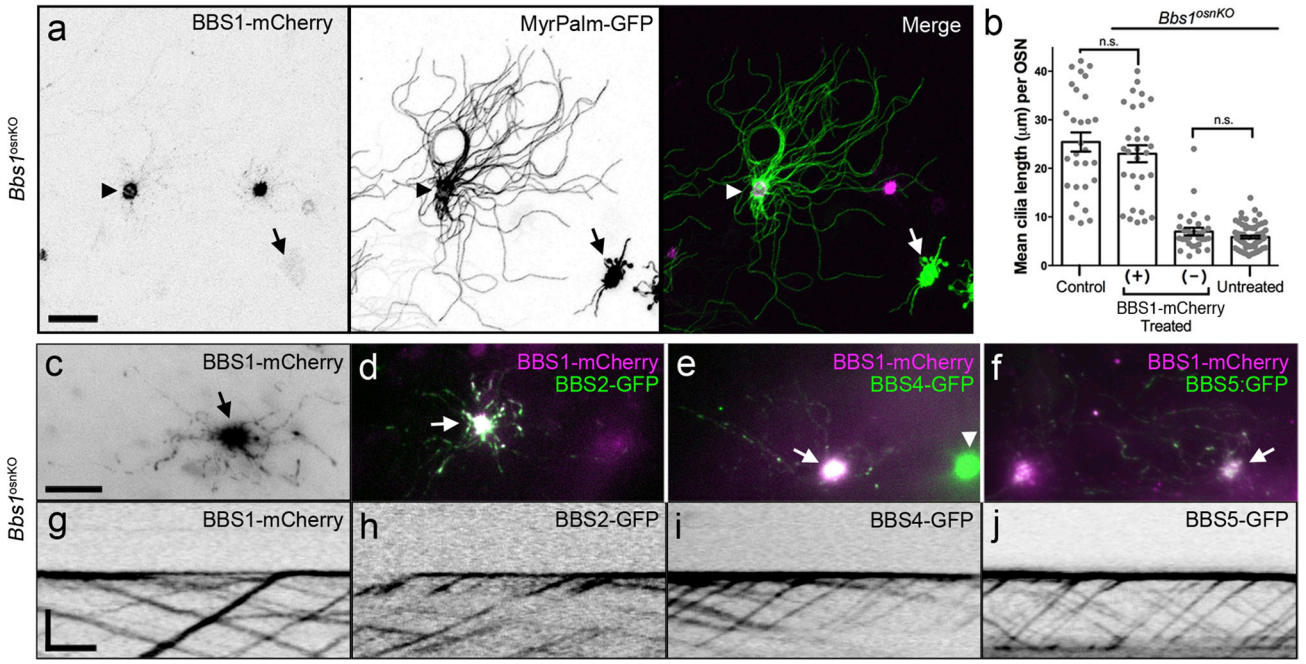

Figure 5. Gene Therapeutic Restoration of Cilium Morphology and BBSome Transport in *Bbs1*^{osnKO} Mutant OSNs

(A and B) Restoration of cilium length in AV-treated OSNs. (A) Representative live en face confocal image showing MyrPalm-GFP-labeled OSN cilia projecting from OSNs expressing BBS1-mCherry (arrowhead) or lack BBS1-mCherry expression (arrows). (B) Quantified data showing restoration of cilium length (based on the MyrPalm-GFP signal) in *Bbs1*^{osnKO} OSNs that ectopically express BBS1-mCherry (+) but not in OSNs that lack BBS1:mCherry (–). No significant difference (n.s.) was seen between the lengths of control OSN cilia and cilia on *Bbs1*^{osnKO} OSNs expressing BBS1-mCherry. In OSNs of AV-treated *Bbs1*^{osnKO} animals that failed to express BBS1-mCherry, cilium length was not significantly different from untreated *Bbs1*^{osnKO} animals. Student's t test, $p > 0.05$. (–F) Restoration of BBSome ciliary localization in AV-treated OSNs. (C) En face TIRF microscopy showed enrichment of the image of BBS1-mCherry in the dendritic knob (arrow) and surrounding cilia, expressed in AV5- BBS1-mCherry-treated *Bbs1*^{osnKO} animals. Ciliary localization of (D) BBS2-GFP, (E) BBS4-GFP, and (F) BBS5-GFP is evident in *Bbs1*^{osnKO} OSNs co-expressing BBS1-mCherry (arrows) but not in OSNs lacking BBS1-mCherry (arrowhead). (G–J) BBSome trafficking is restored in AV-treated OSNs. (G) Kymogram generated from an en face TIRF microscopy time series, displaying bidirectional ciliary trafficking of (H) BBS2-GFP, (I) BBS4-GFP, and (J) BBS5-GFP in cilia from *Bbs1*^{osnKO} OSNs co-expressing BBS1-mCherry (as shown above). Values represent means ± SEM. Scale bars, 10 μm (A and C–F) and 5 μm × 15 s (G–J).

treated with AV5-BBS1-mCherry on post-natal day (P) 7, P8, and P9. Ten days post-treatment, EOG recordings were performed to measure odor responses to varying concentrations and types of odors. Compared with untreated mutants, *Bbs1*^{osnKO} mutants receiving gene therapy showed larger electrical responses to all acutely delivered odors (Figure 6). Remarkably, administration of AV5-BBS1-mCherry was sufficient to restore EOG responses to control levels for tested odors (Figure 6A). Importantly, we also observed the return of EOG responses in treated adult *Bbs1*^{osnKO} mutant animals (ranging from P48–P140) compared with untreated mutants (Figure 6B). Consistent with the responses of the younger rescued animals, EOG recordings from rescued adults were statistically similar to those measured in control adults for tested odors (Figure 6B). Together with increased odorant response in treated animals, we observed partial returns in TH expression and glomerular sizes to control levels within the olfactory bulb (Figures 6C and 6D). Together, our data indicate that intranasal BBS gene therapy can restore odor detection in neonates and adult *Bbs1*^{osnKO} mutant animals to control levels in the periphery and partially restore central activity. Notably, restoration of odor detection in adult animals suggests that BBS mutant OE does not become refractory to gene therapy over time.

Ectopic BBS1 Expression Does Not Lead to Apoptosis or Macrophage Infiltration

In previous reports, ectopic overexpression of BBS1 in control mouse retinas causes tissue damage and cell death.[41] To assess the condition of the OE following ectopic expression of BBS1 in control and *Bbs1*^{osnKO} mutant animals, we quantified apoptosis 10 days after AV5-mCherry or AV5-BBS1-mCherry treatments using cleaved caspase-3 as a marker of apoptosis. In contrast to results from the retinal study, OE morphology appeared normal, and we measured no significant changes in caspase-3-induced apoptotic cell numbers in control or *Bbs1*^{osnKO} mutants treated with AV5-BBS1-mCherry (Figures S5A–S5D), suggesting that overexpression of BBS1 does not compromise the general health of the OE. In addition, we examined macrophage infiltration by IBA-1 immunostaining. Similarly, we did not see significant changes in IBA-1 counts across untreated, AV5-mCherry-treated, and AV5-BBS1-mCherry treated mice (Figures S5E–S5H).

AAV-Mediated Gene Therapy Counteracts *Bbs1*^{osnKO} Mutant Phenotypes

To establish that olfactory BBS gene therapy is feasible with a clinically approved delivery vehicle, we next assessed the potential of

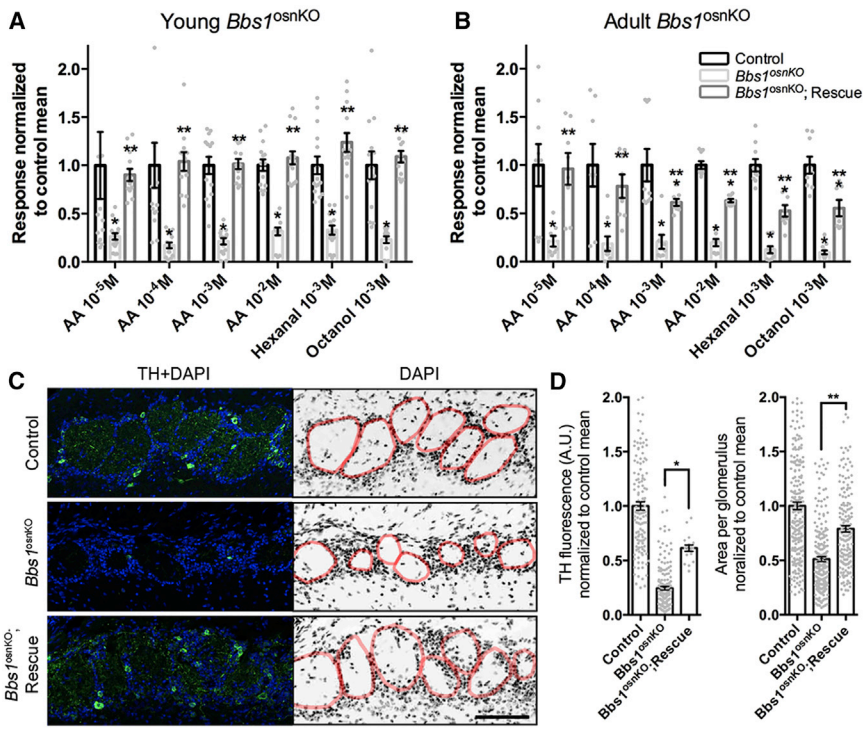

Figure 6. Gene Therapeutic Rescue of Odor Detection in *Bbs1*^{osnKO} Mutants

(A and B) Quantified EOG data showing normalized responses to varying AA concentrations, hexanal, or octanol. (A) Young rescued animals were treated on P7, P8, and P9. (B) Adult rescued animals were treated on 3 consecutive days on or after P36. Compared with untreated mutants, ectopic expression of BBS1-mCherry in *Bbs1*^{osnKO} improved odor detection under all conditions. Student's t test, * significantly different from control, ** rescue significantly different from mutant, $p < 0.05$. (C) Representative confocal images of coronal olfactory bulb slices from young mice showing return of glomerular TH immunoreactivity in rescued *Bbs1*^{osnKO} animals. Right: representative confocal images of DAPI-stained coronal olfactory bulb slices depicting individual glomeruli (red). Glomerular size is increased in rescued *Bbs1*^{osnKO} mutants compared with untreated *Bbs1*^{osnKO} mutants. (D) Left: quantification of mean TH fluorescence increase in rescued compared with untreated *Bbs1*^{osnKO} mutants. One-way ANOVA, $F_{(2,311)} = 38.7$, *$p < 0.001$, Tukey post hoc test. Right: quantification of mean glomerular area increase in rescued *Bbs1*^{osnKO} mutants compared with untreated controls. One-way ANOVA, $F_{(2,586)} = 21.28$, **$p < 0.001$, Tukey post hoc test. Values represent means ± SEM. Scale bar, 100 μm.

adeno-associated virus (AAV) to transduce cells of the OE. We tested several AAV serotypes carrying either GFP or mCherry DNA as fluorescent reporters. We administered a single intranasal viral dose to control mice at age P7 and later assessed reporter expression in fixed coronal OE sections from treated animals. MCherry expression in OSNs (Figure 7A) was observed as early as 24 hr post-treatment and persisted up to 6 weeks. Our data demonstrate that multiple AAV serotypes are capable of transducing the mouse OE, ranging from 5–47 cells/mm (Figure S6). However, compared with the other AAV serotypes, AAV9 exhibited one of the highest specificities toward OSNs, comprising 86% of total transduced cells, at 29.9 OSNs/mm of OE (± 2.3 SEM) (Figure S6). In addition, we examined the spread of intranasal AAV9 infection through live in vivo imaging of AAV9-luciferase expression (Figure 7B). Observed 2 weeks after intranasal administration, luciferase activity was restricted to the nasal cavity. Given these observations, together with the known long-term stability and neurotrophism,[42,43] we chose to use AAV9 for olfactory gene delivery and rescue. *Bbs1*^{osnKO} mutant animals were intranasally treated with WT AAV9-BBS1-mCherry on 3 consecutive days (P7–P9) and were allowed 3 weeks for expression. In fixed coronal OE sections of treated mutants, acetylated α-tubulin immunostaining revealed increased ciliation surrounding BBS1-mCherry-positive OSN dendritic knobs, demonstrating that AAV9 mediated functional expression of BBS1-mCherry in individual cells (Figure 7C). To assess functional rescue by AAV9-BBS1-mCherry on the population level, we measured EOGs on treated animals. Treated animals exhibited increased odorant and odor concentration responses compared with untreated mutants, in most cases equivalent to control levels (Figure 7D). Similar to AV-treated *Bbs1*^{osnKO} mutants, AAV9-BBS1-mCherry treated *Bbs1*^{osnKO} mutants exhibited an increase in TH expression and glomerular sizes compared with untreated mutants (Figures 7E and 7F). Together, these data provide evidence that the olfactory system is amenable to AAV-based gene therapy and that olfactory deficits in BBS mutants can be rescued with this clinically viable approach.

DISCUSSION

In the present study, we demonstrate that gene therapy reverses BBSome-associated defects in the olfactory system. Viral expression of WT BBS proteins increased cilium length and the number on individual OSNs and restored acute odor response at the tissue level. Notably, our approach used non-invasive techniques and promoted biogenesis or repair of organelles in mature sensory neurons across the OE. Importantly, this is the initial report of gene therapeutic recovery in a model system that represents a treatable human cohort suffering from olfactory deficits. We demonstrated that a BBS mutant model affecting the BBSome was amenable to rescue, suggesting that clinical gene therapeutic strategies may be effective across the general BBS patient population. In addition, the generation and analysis of the OSN-specific *Bbs1* knockout enabled isolation of the peripheral olfactory system as the primary source of olfactory impairment in BBS mutants and ruled out a causative role of impaired odor detection in the obesity phenotype in BBS. This is also the first model in which a ciliary gene was selectively disrupted in the principal sensory cells of the OE. In future studies examining the effect of sensory deprivation on the olfactory circuit, the use of the OSN-specific knockout will be

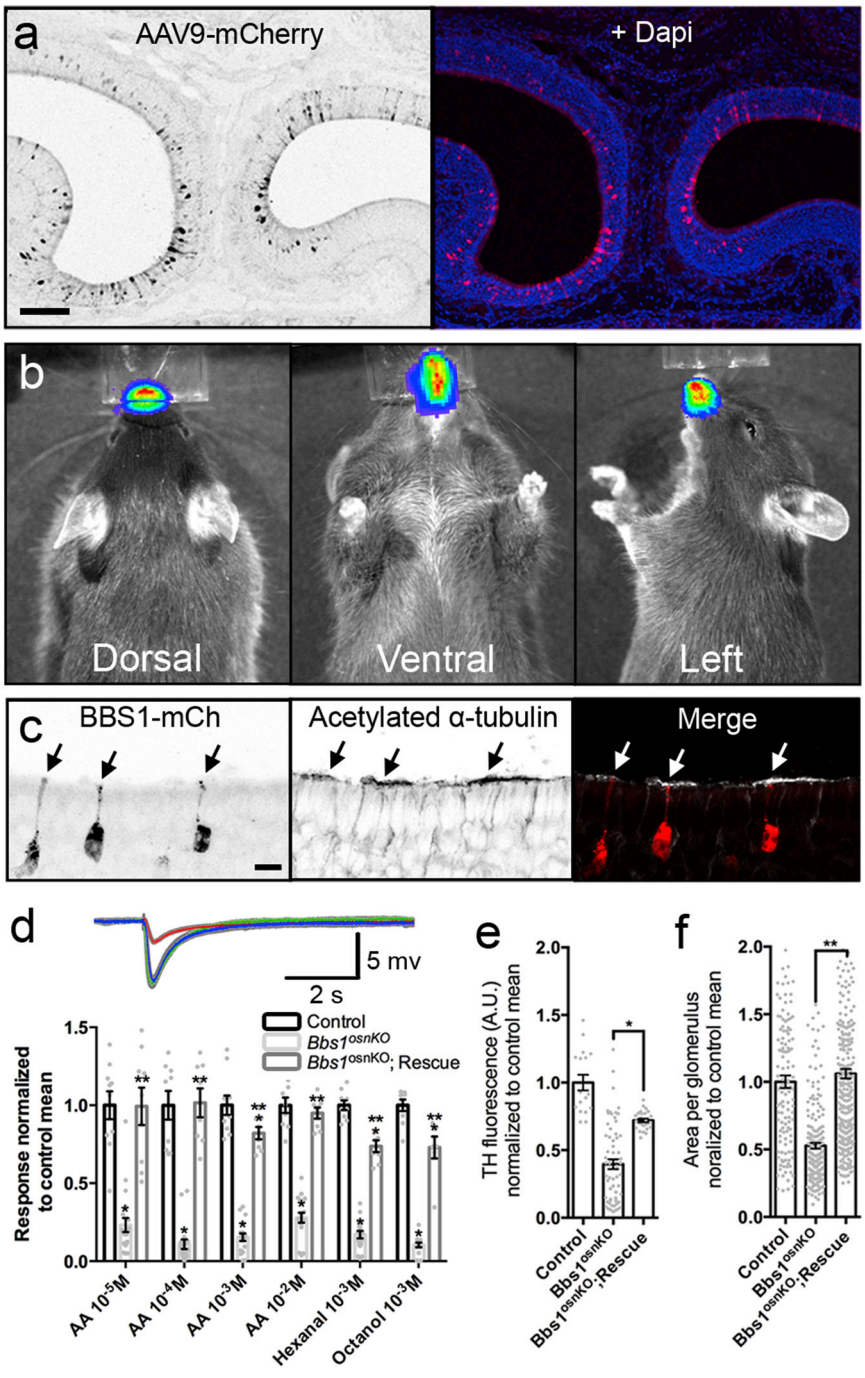

Figure 7. AAV9-Mediated Rescue of Ciliation and Odor Detection in *Bbs1*^{osnKO} Mutants

(A) Representative confocal image showing a fixed coronal OE section from a control animal 6 days after AVV9-mediated mCherry delivery. (B) Representative in vivo images showing restriction of infection to the nasal cavity of a control animal 14 days after AAV9-mediated luciferase delivery. (C) AAV9-BBS1-mCherry restores OSN ciliary microtubules in *Bbs1*^{osnKO} animals. The representative image shows a fixed coronal section of OE from a *Bbs1*^{osnKO} mutant 3 weeks after treatment with AAV9-BBS1-mCherry, immunostained for acetylated α-tubulin. Acetylated α-tubulin signal intensity is locally increased in the immediate proximity of dendritic knobs (arrows) projecting from AAV-transduced OSNs. (D) Top: representative EOG recordings from the OE surface of the control (green), *Bbs1*^{osnKO} mutant (red), and BBS1:mCherry-treated *Bbs1*^{osnKO} mutant (blue) in response to 10^{-3} M amyl acetate. Bottom: quantified EOG data showing normalized responses to varying AA concentrations, hexanal, or octanol. Rescue animals were treated on P7, P8, and P9 and tested on P38. Compared with untreated mutants, AAV9-BBS1-mCherry-treated *Bbs1*^{osnKO} mutants showed improved odor detection. Student's t test, * significantly different from control, ** rescue significantly different from mutant, $p < 0.05$. (E) Quantification of mean TH fluorescence increased in AAV9-BBS1:mCherry-treated compared with untreated *Bbs1*^{osnKO} mutants. One-way ANOVA, $F_{(2,104)} = 16.26$, *$p < 0.001$, Tukey post hoc test. (F) Quantification of mean glomerular area increase in rescued *Bbs1*^{osnKO} mutants compared with untreated controls. One-way ANOVA, $F_{(2,613)} = 30.12$, **$p < 0.001$, Tukey post hoc test. Values represent means ± SEM. Scale bars, 100 μm (A), 10 μm (C), and 5 mV × 5 s (D).

useful over previous global cilium gene knockouts in which interpretation of downstream olfactory phenotypes could be clouded by contributions from other mutant cell types.

Our data demonstrate that both AVs and AAVs are capable of transducing cells within the nasal epithelium, opening the door for the development of clinical gene therapeutic treatments for peripheral olfactory disorders. Indeed, ectopic AV5 and AAV9-mediated gene expression occurred early in the OE and was sustained over the duration of our analysis (10 days for AV5 and 3–6 weeks for AAVs). We demonstrated that AVs and AAVs have the ability to infect OSNs, with AAV9 exhibiting preferences for neurons. In this regard, infection specificity and efficiency could be further improved by the incorporation of neuronal or OSN-specific promoters within the viral vectors, a strategy previously implemented in other cell and tissue types.[44,45] Intranasal delivery of WT AV5 and AAV9-BBS1 was sufficient for cilium restoration on individual neurons, restoration of BBSome trafficking, and improved odor detection, bypassing the complications of systemic delivery.[46,47] Using this approach, we induced partial return of TH expression and glomerular sizes within the olfactory bulb, which is indicative of restored afferent innervation and activity;[35,48,49] however, additional anatomical and functional studies are required to determine whether axonal convergence and

odorant processing at the level of the olfactory bulb are reestablished in rescued *Bbs1*^{osnKO} mice. We estimated that our non-invasive method induced ectopic gene expression in roughly 15% of mature OSNs. This infection efficiency is surprising because it implies that a modest number of functional OSNs are sufficient for acute odor detection and central connectivity. Although previous reports in *Rana pipiens* showed that recovery from global cilium lesion with detergent correlated with the return of EOG responses,[50] our results imply a significant spare capacity for odor detection requiring only a subset of functional neurons. In the future, the relationship between the number of transduced cells and increment of odorant concentration responses should be considered. Nonetheless, these observations are encouraging because the treatment achieved measurable restoration of olfactory sensitivity without necessitating high infection efficiency, suggesting that a similar approach in patients may elicit positive initial outcomes.

Notably, our treatment paradigm was effective in both young and adult animals, suggesting that age is not a major limiting factor for gene therapy efficacy in the OE of *Bbs1*^{osnKO} mutant mice. This finding suggests a broad therapeutic window for initiation of clinical treatment, especially given the limited diagnostic tools for assessing olfactory function in patients. This is contradictory to other afflicted tissues, such as the retina, where BBS patients and animal models experience progressive photoreceptor cell loss over time.[25,51–53] Because of persistent cell degradation, BBS gene therapy efficacy in the rodent retina has largely been focused on preventative treatment in young animals.[54] Unlike photoreceptors, OSNs do not experience excessive degeneration in the absence of stimulation, and older or damaged OSNs are constantly replaced by new neurons from a population of neuronal stem cells within the OE.[55] Because sensory-incompetent but otherwise healthy OSNs persist in *Bbs1*^{osnKO} mutant mice, we were able to target a stable population of mature neurons and induce the regeneration of their sensory organelles to restore/enable odor detection.

Compared to AVs, AAVs are advantageous because of their low immunogenicity[56] and the capacity to stably incorporate vector DNA into the host genome,[57–59] suggesting persistent expression in treated OSNs. However, OSNs undergo constant turnover, with the lifespan of individual neurons ranging between 60–90 days.[60,61] Therefore, targeting the underlying immature OSNs and aforementioned basal stem cells may allow for a more prolonged or permanent therapeutic strategy. Our current intranasal delivery with either vector limits infection to cells exposed to the apical surface of the OE, with no observed co-localization of mCherry signal in the basal stem cell population. AAV infection of deeper cells may be inhibited in part by the presence of tight junctions at the apical surface of the OE.[62,63] This could be circumvented by partial ablation of the OE to disrupt the tight junctions and expose the basal stem cell population.[64–67] Another possible way to transduce deeper layers of OE is the addition of adjuvants to permeabilize epithelial tight junctions. Pretreatment of airway epithelia with sodium caprate increased AV-mediated gene expression in deeper layers by opening tight junctions.[68,69] Similarly, pretreatment with other adjuvants such as lysophosphatidylcholine, a natural surfactant component, and polyethylenimine, a cationic polymer, improved in vivo transduction of ciliated cells with lentiviral vectors.[70–72] Besides access from the apical surface, the basal stem cells could be targeted from the basolateral surface through the lamina propria but would require either systemic administration or local injection of the AAV. Regardless, targeting the basal stem cell population would necessitate methodologies that would limit prolonged tissue damage while maintaining regional and tissue specificity.

The autosomal recessive mode of inheritance in ciliopathies is compatible with gene therapeutic strategies that compensate for homozygous loss-of-function alleles. Although BBS is classically autosomal-recessive, some BBS patient alleles express dominant-negative phenotypes in heterologous systems.[73] The existence of these phenotypes necessitates an understanding of the pathogenicity of individual patient alleles prior to proceeding with personalized treatments. Detrimental effects from overexpression may become obstacles in developing treatment paradigms that feature ectopic BBS gene delivery. Ectopic AAV-mediated overexpression of WT BBS1 in WT retinas, but not in *Bbs1* mutant retinas, causes tissue toxicity, and treated mutant retinas show only minimal functional rescue.[41] In contrast, we observed no caspase-3-induced apoptotic effects or macrophage infiltration from AV-mediated WT BBS1 overexpression in the OE of control animals, and odor detection was most often restored to control levels in treated mutant animals; however, BBS protein overexpression toxicity in the olfactory system must be assessed in the context of the BBS1 (M390R) missense mutation as well as other BBS loss-of-function mutations. The differences between the retina and OE may reflect a stronger capacity of the OE to tolerate overexpression because we previously observed no overexpression-related pathogenicity of basal body, transition zone, axoneme, IFT, BBS, or polytopic signaling proteins in WT OE.[14]

Loss of BBS1 drastically reduced OSN ciliation in the OE with decreased cilium length and number. However, the persistence of residual cilia allowed for the unique examination of cilium protein trafficking and BBSome functional analysis in intact multiciliated cells. Although BBS1 is generally not required for BBSome complex assembly in cultured cells,[34] we found that BBS1 is essential for BBSome translocation into OSN cilia. Interestingly, the residual OSN cilia in *Bbs1*^{osnKO} mutants retained the capacity of bidirectional IFT, but the degree to which it affects protein trafficking dynamics remains unclear. Evidence from *C. elegans* suggests a link between BBSome function and IFT particle velocity.[74] BBS1 loss of function mutations in *C. elegans* mutants assume faster IFT-B velocities but slower IFT-A velocities based on associations with homodimeric kinesin (OSM-3) and heterotrimeric kinesin 2, respectively.[75,76] In addition, a growing body of evidence suggests that BBSome function is required for retrograde export of ciliary membrane proteins.[8,17,77,78] The BBSome directly interacts with several ciliary membrane proteins, including somatostatin receptor 3, polycystin 2, patched, and smoothened.[11,78,79] Loss of BBS1 may lead to decoupling of the BBSome to one or more of the membrane

protein cargoes, potentially altering the IFT particle composition and velocities. Nonetheless, a detailed mechanistic study of BBS1 loss and its rescue on OSN ciliary trafficking dynamics warrants further investigation.

In summary, our work has uncovered novel olfactory cilium biogenesis/maintenance and trafficking phenotypes associated with the disruption of mammalian BBS proteins that can be corrected via ectopic gene delivery. Importantly, this is the first report of gene therapy rectifying olfactory deficits in a model system corresponding to a treatable patient population. Moreover, our demonstration of AAV transduction and functional rescue in the OE brings the olfactory system within the realm of tissues/organs that have the capacity to undergo clinical gene therapeutic treatments. Our positive results in the olfactory system with the OSN-specific BBS1 knockout line, coupled with successful implementation of gene therapy in the retina,[54] suggests that additional tissues of BBS patients will also be amenable to corrective treatments.

MATERIALS AND METHODS

Mice

The floxed *Bbs1* allele was provided by V.C. Sheffield. The *OMP-Cre* allele was acquired from The Jackson Laboratory. Floxed *Bbs1;OMP-Cre* animals were of mixed genetic background. OMP-GFP and C57BL/6 mice were acquired from The Jackson Laboratory. All mice were housed at the University of Florida. All procedures were approved by the University of Florida Institutional Animal Care and Use Committee. For genotyping, DNA was extracted from tail clippings with Extracta DNA Prep for PCR – Tissue (Quanta Biosciences) and amplified with GoTaq Green Mastermix (Promega).

Immunohistochemistry

Mice were deeply anesthetized prior to cardiac perfusion with 4% paraformaldehyde (PFA). Dissected snouts were then incubated in 4% PFA overnight at 4°C. Following decalcification in 0.5 M EDTA/1× PBS overnight, snouts were cryoprotected in 10%, 20%, and 30% sucrose in 1× PBS for 1 hr, 1 hr, and overnight, respectively, at 4°C, and embedded in optimal cutting temperature (OCT) compound (Tissue-tek). Embedded tissues were cryosectioned along the coronal plane at a thickness of 10–12 μm and mounted onto Superfrost Plus slides (Fisher Scientific). For immunostaining, cryosections were permeabilized and blocked with 0.1% Triton X-100 and 2% goat serum in 1× PBS for 30 min. Primary antibodies were diluted in 2% goat serum and applied to samples for 1 hr at room temperature. When multiple primary antibodies were used, incubations with each antibody were performed sequentially, and samples were washed three times with 1× PBS between each incubation. Primary antibodies were used at the following concentrations: acetylated α-tubulin (clone 6-11 B-1 #T6793, Sigma), 1:1,000; OMP (544-10001, Wako), 1:1,000; ACIII (C-20, sc-588, Santa Cruz Biotechnology), 1:1,000; Cnga2 (#APC-045, Alomone Labs), 1:1,000; tyrosine hydroxylase (MAB318, Millipore), 1:500; cleaved caspase-3 (Asp175, Cell Signaling Technology), 1:400; and IBA-1 (#ab5076, Abcam), 1:500. Fluorescently conjugated secondary antibodies were applied (at 1:1,000 dilution) for 1 hr, and sections were then washed three times with PBS. DAPI was applied for 5 min to stain nuclei, and samples were mounted using Prolong Gold (Invitrogen). Fixed tissue imaging was performed on a Nikon TiE-PFS-A1R confocal microscope equipped with a 488-nm laser diode with a 510- to 560-nm band-pass filter and 561 laser with a 575- to 625-nm band-pass filter. A CFI Apochromat Lamda S 60 × 1.4 N.A. objective was used. Confocal z stacks were processed using NIH ImageJ software and assembled in Adobe Photoshop CS and Adobe Illustrator CS.

Scanning Electron Microscopy

Mice were placed under deep anesthesia and subjected to cardiac perfusion with 2% glutaraldehyde and 0.15 M cacodylate in water. Olfactory turbinates were dissected and processed using the osmium tetroxide (OsO4)/thiocarbohydrazide (OTOTO) protocol. Analysis was performed on an Amray 1910FE field emission scanning electron microscope (Drogheda) at 5 kV and recorded digitally with Semicaps software.

Vectors

Plasmids containing mouse cDNA fragments were provided as follows: ACIII (R. Reed, Johns Hopkins); BBS1, BBS2, BBS3, and BBS5 (K. Mykytyn, The Ohio State University); Efhc1 (K. Yamakawa, RIKEN), IFT88 (B.K. Yoder, University of Alabama at Birmingham); IFT122 (J. Eggenschwiler, University of Georgia); and Kap3a (T. Schroer, Johns Hopkins University). MyrPalm-GFP and Dync2li1-GFP were described previously.[14] All cDNAs were fused with GFP or mCherry and inserted into the pAd/CMV/V5-DEST expression vector using Gateway technology (Invitrogen). Adenoviral vectors were propagated using the ViraPower protocol (Invitrogen), isolated with the Virapur Adenovirus mini purification Virakit, and dialyzed in 2.5% glycerol, 25 mM NaCl, and 20 mM Tris-HCl (pH 8.0) with a Slide-A-Lyzer dialysis cassette (Thermo Scientific). For production of AAV9-BBS1-mCherry, BBS1-mCherry DNA was subcloned into the pUF11 rAAV vector, which drives expression via the chicken β-actin promoter. pUF11-BBS1:mCherry was packaged in AAV9 and titered by the Vector Core of the Powell Gene Therapy Center (University of Florida) using previously described methods.[80] AAV9-mCherry was provided by the Powell Gene Therapy Center.

Ectopic Gene Delivery

Standard viral vector gene delivery involves the administration of 20 μL of virus on 3 consecutive days and examination 10 days after the third treatment. During and after treatment days, mice were closely monitored for alertness and health. For young animal experiments, 20-μL AV doses were administered directly to the nasal cavity of unanesthetized, pups at P7, P8, and P9. For adult animal experiments (on or after P36), mice were lightly anesthetized with isoflurane and received 20-μL doses on 3 consecutive days. For all mice, viral delivery was performed by a pulled 1-mL syringe (~0.5-mm tip) placed at the nostrils and administered during each inhalation. Pups receiving AAV9-mCherry were given a single intranasal 10-μL dose at P7, and pups receiving AAV9-BBS1-mCherry were given 10-μL doses at P7, P8, and P9. AAV9-mCherry and AAV9-BBS1-mCherry

were administered at 2.32 × 10^{12} and 1.91 × 10^{12} vector genomes (vg)/mL, respectively.

En Face Imaging

For confocal imaging, virally transduced animals were anesthetized with CO_2, rapidly decapitated, and split along the cranial midline, and then the olfactory turbinates were exposed by removing any remaining septal tissue. The rostral- and caudal-most portions of one hemisection were removed, leaving the olfactory epithelium and olfactory bulb intact in the skull. The tissue was placed turbinate surface down in a bath of 1× PBS in the imaging chamber and held in place with mesh netting. Samples were placed in a tissue chamber and imaged on a Nikon TiE-PFS-A1R confocal microscope (described above). For TIRF microscopy imaging, virally transduced animals were prepared as above, with the exception of 1× PBS being replaced by 35°C artificial cerebrospinal fluid (ACSF; 124 mM NaCl, 3 mM KCL, 1 mM $MgCl_2$, 2 mM $CaCl_2$, 1.25 mM NaH_2PO_4, 26 mM $NaHCO_3$, and 25 mM glucose) bubbled with 5% CO_2/95% O_2 for at least 10 min prior to use. TIRF microscopy time series were captured at 200-ms exposure with a zero delay interval for 2–3 min on a Nikon Eclipse Ti-E/B inverted microscope equipped with a 100× CFI Apochromat TIRF 1.49 N.A., 1.5× tube lens, ZT488/561rpc dichroic, ZET488/561x excitation filter, ZET488/561m-TRF emission filter (Chroma Technology), and an electron multiplying charge-coupled device (EMCCD) camera (iXon X3 DU897, Andor Technology). The 488-nm line of a fiber-coupled diode laser at an incident power of 2 MW was used to illuminate a circular region of ~60 μm in diameter for capturing video sequences at 5–10 Hz. ImageJ was used to generate line scan kymograms for visualizing particle movement from imported time series.

OSN Cilium Measurements

Tissues were prepared according to en face confocal imaging, with turbinate T1 removed during dissections. The olfactory epithelium along the turbinate surface was divided based on the natural borders delineating turbinates T2a, T2b, T3, and T4 from rostral to caudal according to Figure S3A. The turbinates and their borders were identified through the eyepiece (10× magnification) under epifluorescence prior to imaging. Individual or clusters of OSNs with intact cilia were identified based on AV-mediated ectopic expression of MyrPalm-GFP or MyrPalm-mCherry. Confocal z stack images of identified OSNs were collected at either 40× or 60× magnifications. Cilium length measurements and counts were performed independently on ImageJ by individuals blind to mouse genotype, treatment conditions, and turbinate location. The resulting measurements were subsequently compiled and analyzed by C.L.W. and C.R.U.

Electro-olfactograms

Mice were anesthetized with CO_2, rapidly decapitated, and split along the cranial midline. Septal tissue was removed to expose the olfactory turbinates. Vapor-phase odor stimuli were generated by placing 10 mL of odors diluted in water in a sealed 100-mL glass bottle. Odorants were delivered as a 100-ms pressurized pulse injected into a continuous stream of humidified air flowing over the tissue using a picospritzer controlled by Clampex software. Electrodes (1–4 MOhm) were made of borosilicate glass capillaries filled with 0.5% SeaPlaque agarose (Lonza) in modified Ringer's solution (135 mM NaCl, 5 mM KCl, 1 mM $CaCl_2$, 1.5 mM $MgCl_2$, and 10 mM HEPES, pH 7.4) and positioned for recording on olfactory turbinates IIa or IIb. Responses to odor stimuli were recorded with a Multiclamp amplifier controlled by Clampex and analyzed with Clampfit (pClamp10.2, Molecular Devices). Responses were measured as peak changes from the pre-pulse baseline. At least three mice were tested for each condition.

In Vivo Imaging of Bioluminescence

C57BL/6 mice (n = 3) of age P8 were administered the rAAV2/9 vector carrying luciferase (S. Zolotukhin, University of Florida). A single dose of 10 μL of virus with a titer of 10^{12} vg/mL was applied as described for AV vector administration. Mice were imaged 14 days later using the Xenogen IVIS system (PerkinElmer). Mice were anesthetized with isoflurane, intraperitoneally injected with 15 mg/mL of XenoLight potassium salt of D-luciferin (PerkinElmer) dissolved in sterile divalent-free Dulbecco's PBS, and imaged between 5 and 20 min after the injection. To assess the difference in bioluminescence distribution, animals were viewed in the ventral, dorsal, and lateral positions. Acquired images were analyzed and saved as TIFF files using Living Image software (PerkinElmer).

SUPPLEMENTAL INFORMATION

Supplemental Information includes six figures and can be found with this article online at http://dx.doi.org/10.1016/j.ymthe.2017.02.006.

AUTHOR CONTRIBUTIONS

C.L.W. and J.R.M. designed the experiments. C.L.W., C.R.U., A.D.Z., D.T.S., and K.U. performed the experiments. C.L.W., J.C.M, W.W.G., and L.Z. generated the reagents. V.C.S. and D.Y.N. designed and developed the mouse models of BBS. C.L.W., C.R.U., and J.R.M. wrote the manuscript, with all authors providing input. C.L.W. and C.R.U. generated the figures. J.R.M. directed the project.

CONFLICTS OF INTEREST

The authors declare no conflict of interest.

ACKNOWLEDGMENTS

We thank L. Bayer and A. Dinculescu for technical assistance and C. Searby for assistance with generating the mouse models. AAV9 luciferase was provided by S. Zolotukhin. In vivo imaging was performed in the University of Florida Imaging Core. K. Ukhanov, W. Green, and S. Munger provided helpful criticism of the manuscript, and further intellectual support was provided by A. Joiner, J. McIntyre, and members of the University of Florida Center for Smell and Taste. This work was supported by R01DC009606 (to J.R.M.), F32DC011990 (to J.C.M.), and R01EY11298 (to V.C.S.).

REFERENCES

1. Badano, J.L., Mitsuma, N., Beales, P.L., and Katsanis, N. (2006). The ciliopathies: an emerging class of human genetic disorders. Annu. Rev. Genomics Hum. Genet. *7*, 125–148.

2. Forsythe, E., and Beales, P.L. (2013). Bardet-Biedl syndrome. Eur. J. Hum. Genet. *21*, 8–13.

3. Sheffield, V.C., ZQ, Heon, E., Drack, A., and Stone, E.M. (2016). The Bardet-Biedl Syndrome. In Epstein's Inborn Errors of Development: The Molecular Basis of Clinical Disorders of Morphogensis, Chapter 3 – Defined Core Developmental Pathways Linked to Cilia, 3rd edition, R.P. Erickson and A.J. Wynshaw-Boris, eds. (Oxford University Press), pp. 237–240.

4. Kulaga, H.M., Leitch, C.C., Eichers, E.R., Badano, J.L., Lesemann, A., Hoskins, B.E., Lupski, J.R., Beales, P.L., Reed, R.R., and Katsanis, N. (2004). Loss of BBS proteins causes anosmia in humans and defects in olfactory cilia structure and function in the mouse. Nat. Genet. *36*, 994–998.

5. Braun, J.J., Noblet, V., Durand, M., Scheidecker, S., Zinetti-Bertschy, A., Foucher, J., Marion, V., Muller, J., Riehm, S., Dollfus, H., and Kremer, S. (2014). Olfaction evaluation and correlation with brain atrophy in Bardet-Biedl syndrome. Clin. Genet. *86*, 521–529.

6. Nachury, M.V., Loktev, A.V., Zhang, Q., Westlake, C.J., Peränen, J., Merdes, A., Slusarski, D.C., Scheller, R.H., Bazan, J.F., Sheffield, V.C., and Jackson, P.K. (2007). A core complex of BBS proteins cooperates with the GTPase Rab8 to promote ciliary membrane biogenesis. Cell *129*, 1201–1213.

7. Berbari, N.F., Lewis, J.S., Bishop, G.A., Askwith, C.C., and Mykytyn, K. (2008). Bardet-Biedl syndrome proteins are required for the localization of G protein-coupled receptors to primary cilia. Proc. Natl. Acad. Sci. USA *105*, 4242–4246.

8. Domire, J.S., Green, J.A., Lee, K.G., Johnson, A.D., Askwith, C.C., and Mykytyn, K. (2011). Dopamine receptor 1 localizes to neuronal cilia in a dynamic process that requires the Bardet-Biedl syndrome proteins. Cell. Mol. Life Sci. *68*, 2951–2960.

9. Loktev, A.V., and Jackson, P.K. (2013). Neuropeptide Y family receptors traffic via the Bardet-Biedl syndrome pathway to signal in neuronal primary cilia. Cell Rep. *5*, 1316–1329.

10. Seo, S., Zhang, Q., Bugge, K., Breslow, D.K., Searby, C.C., Nachury, M.V., and Sheffield, V.C. (2011). A novel protein LZTFL1 regulates ciliary trafficking of the BBSome and Smoothened. PLoS Genet. *7*, e1002358.

11. Jin, H., White, S.R., Shida, T., Schulz, S., Aguiar, M., Gygi, S.P., Bazan, J.F., and Nachury, M.V. (2010). The conserved Bardet-Biedl syndrome proteins assemble a coat that traffics membrane proteins to cilia. Cell *141*, 1208–1219.

12. Liew, G.M., Ye, F., Nager, A.R., Murphy, J.P., Lee, J.S., Aguiar, M., Breslow, D.K., Gygi, S.P., and Nachury, M.V. (2014). The intraflagellar transport protein IFT27 promotes BBSome exit from cilia through the GTPase ARL6/BBS3. Dev. Cell *31*, 265–278.

13. Rosenbaum, J.L., and Witman, G.B. (2002). Intraflagellar transport. Nat. Rev. Mol. Cell Biol. *3*, 813–825.

14. Williams, C.L., McIntyre, J.C., Norris, S.R., Jenkins, P.M., Zhang, L., Pei, Q., Verhey, K., and Martens, J.R. (2014). Direct evidence for BBSome-associated intraflagellar transport reveals distinct properties of native mammalian cilia. Nat. Commun. *5*, 5813.

15. Fan, Y., Esmail, M.A., Ansley, S.J., Blacque, O.E., Boroevich, K., Ross, A.J., Moore, S.J., Badano, J.L., May-Simera, H., Compton, D.S., et al. (2004). Mutations in a member of the Ras superfamily of small GTP-binding proteins causes Bardet-Biedl syndrome. Nat. Genet. *36*, 989–993.

16. Blacque, O.E., Reardon, M.J., Li, C., McCarthy, J., Mahjoub, M.R., Ansley, S.J., Badano, J.L., Mah, A.K., Beales, P.L., Davidson, W.S., et al. (2004). Loss of C. elegans BBS-7 and BBS-8 protein function results in cilia defects and compromised intraflagellar transport. Genes Dev. *18*, 1630–1642.

17. Lechtreck, K.F., Johnson, E.C., Sakai, T., Cochran, D., Ballif, B.A., Rush, J., Pazour, G.J., Ikebe, M., and Witman, G.B. (2009). The Chlamydomonas reinhardtii BBSome is an IFT cargo required for export of specific signaling proteins from flagella. J. Cell Biol. *187*, 1117–1132.

18. Tadenev, A.L., Kulaga, H.M., May-Simera, H.L., Kelley, M.W., Katsanis, N., and Reed, R.R. (2011). Loss of Bardet-Biedl syndrome protein-8 (BBS8) perturbs olfactory function, protein localization, and axon targeting. Proc. Natl. Acad. Sci. USA *108*, 10320–10325.

19. McIntyre, J.C., Williams, C.L., and Martens, J.R. (2013). Smelling the roses and seeing the light: gene therapy for ciliopathies. Trends Biotechnol. *31*, 355–363.

20. Ross, A.J., May-Simera, H., Eichers, E.R., Kai, M., Hill, J., Jagger, D.J., Leitch, C.C., Chapple, J.P., Munro, P.M., Fisher, S., et al. (2005). Disruption of Bardet-Biedl syndrome ciliary proteins perturbs planar cell polarity in vertebrates. Nat. Genet. *37*, 1135–1140.

21. M'hamdi, O., Ouertani, I., and Chaabouni-Bouhamed, H. (2014). Update on the genetics of bardet-biedl syndrome. Mol. Syndromol. *5*, 51–56.

22. McIntyre, J.C., Davis, E.E., Joiner, A., Williams, C.L., Tsai, I.C., Jenkins, P.M., McEwen, D.P., Zhang, L., Escobado, J., Thomas, S., et al.; NISC Comparative Sequencing Program (2012). Gene therapy rescues cilia defects and restores olfactory function in a mammalian ciliopathy model. Nat. Med. *18*, 1423–1428.

23. Chamling, X., Seo, S., Bugge, K., Searby, C., Guo, D.F., Drack, A.V., Rahmouni, K., and Sheffield, V.C. (2013). Ectopic expression of human BBS4 can rescue Bardet-Biedl syndrome phenotypes in Bbs4 null mice. PLoS ONE *8*, e59101.

24. Davis, R.E., Swiderski, R.E., Rahmouni, K., Nishimura, D.Y., Mullins, R.F., Agassandian, K., Philp, A.R., Searby, C.C., Andrews, M.P., Thompson, S., et al. (2007). A knockin mouse model of the Bardet-Biedl syndrome 1 M390R mutation has cilia defects, ventriculomegaly, retinopathy, and obesity. Proc. Natl. Acad. Sci. USA *104*, 19422–19427.

25. Fath, M.A., Mullins, R.F., Searby, C., Nishimura, D.Y., Wei, J., Rahmouni, K., Davis, R.E., Tayeh, M.K., Andrews, M., Yang, B., et al. (2005). Mkks-null mice have a phenotype resembling Bardet-Biedl syndrome. Hum. Mol. Genet. *14*, 1109–1118.

26. Nishimura, D.Y., Fath, M., Mullins, R.F., Searby, C., Andrews, M., Davis, R., Andorf, J.L., Mykytyn, K., Swiderski, R.E., Yang, B., et al. (2004). Bbs2-null mice have neurosensory deficits, a defect in social dominance, and retinopathy associated with mislocalization of rhodopsin. Proc. Natl. Acad. Sci. USA *101*, 16588–16593.

27. Carter, C.S., Vogel, T.W., Zhang, Q., Seo, S., Swiderski, R.E., Moninger, T.O., Cassell, M.D., Thedens, D.R., Keppler-Noreuil, K.M., Nopoulos, P., et al. (2012). Abnormal development of NG2+PDGFR-α+ neural progenitor cells leads to neonatal hydrocephalus in a ciliopathy mouse model. Nat. Med. *18*, 1797–1804.

28. Li, J., Ishii, T., Feinstein, P., and Mombaerts, P. (2004). Odorant receptor gene choice is reset by nuclear transfer from mouse olfactory sensory neurons. Nature *428*, 393–399.

29. Menco, B.P. (1997). Ultrastructural aspects of olfactory signaling. Chem. Senses *22*, 295–311.

30. Strotmann, J., Levai, O., Fleischer, J., Schwarzenbacher, K., and Breer, H. (2004). Olfactory receptor proteins in axonal processes of chemosensory neurons. J. Neurosci. *24*, 7754–7761.

31. Menco, B.P. (1980). Qualitative and quantitative freeze-fracture studies on olfactory and nasal respiratory epithelial surfaces of frog, ox, rat, and dog. II. Cell apices, cilia, and microvilli. Cell Tissue Res. *211*, 5–29.

32. Menco, B.P. (1980). Qualitative and quantitative freeze-fracture studies on olfactory and nasal respiratory structures of frog, ox, rat, and dog. I. A general survey. Cell Tissue Res. *207*, 183–209.

33. Katoh, Y., Nozaki, S., Hartanto, D., Miyano, R., and Nakayama, K. (2015). Architectures of multisubunit complexes revealed by a visible immunoprecipitation assay using fluorescent fusion proteins. J. Cell Sci. *128*, 2351–2362.

34. Zhang, Q., Yu, D., Seo, S., Stone, E.M., and Sheffield, V.C. (2012). Intrinsic protein-protein interaction-mediated and chaperonin-assisted sequential assembly of stable bardet-biedl syndrome protein complex, the BBSome. J. Biol. Chem. *287*, 20625–20635.

35. Baker, H., Kawano, T., Margolis, F.L., and Joh, T.H. (1983). Transneuronal regulation of tyrosine hydroxylase expression in olfactory bulb of mouse and rat. J. Neurosci. *3*, 69–78.

36. Zheng, C., Feinstein, P., Bozza, T., Rodriguez, I., and Mombaerts, P. (2000). Peripheral olfactory projections are differentially affected in mice deficient in a cyclic nucleotide-gated channel subunit. Neuron *26*, 81–91.

37. Zou, D.J., Chesler, A.T., Le Pichon, C.E., Kuznetsov, A., Pei, X., Hwang, E.L., and Firestein, S. (2007). Absence of adenylyl cyclase 3 perturbs peripheral olfactory projections in mice. J. Neurosci. *27*, 6675–6683.

38. Baker, H., Morel, K., Stone, D.M., and Maruniak, J.A. (1993). Adult naris closure profoundly reduces tyrosine hydroxylase expression in mouse olfactory bulb. Brain Res. *614*, 109–116.

39. Coppola, D.M. (2012). Studies of olfactory system neural plasticity: the contribution of the unilateral naris occlusion technique. Neural Plast. *2012*, 351752.

40. Davenport, J.R., Watts, A.J., Roper, V.C., Croyle, M.J., van Groen, T., Wyss, J.M., Nagy, T.R., Kesterson, R.A., and Yoder, B.K. (2007). Disruption of intraflagellar transport in adult mice leads to obesity and slow-onset cystic kidney disease. Curr. Biol. *17*, 1586–1594.

41. Seo, S., Mullins, R.F., Dumitrescu, A.V., Bhattarai, S., Gratie, D., Wang, K., Stone, E.M., Sheffield, V., and Drack, A.V. (2013). Subretinal gene therapy of mice with Bardet-Biedl syndrome type 1. Invest. Ophthalmol. Vis. Sci. *54*, 6118–6132.

42. Limberis, M.P., and Wilson, J.M. (2006). Adeno-associated virus serotype 9 vectors transduce murine alveolar and nasal epithelia and can be readministered. Proc. Natl. Acad. Sci. USA *103*, 12993–12998.

43. Dayton, R.D., Wang, D.B., and Klein, R.L. (2012). The advent of AAV9 expands applications for brain and spinal cord gene delivery. Expert Opin. Biol. Ther. *12*, 757–766.

44. Lee, Y., Messing, A., Su, M., and Brenner, M. (2008). GFAP promoter elements required for region-specific and astrocyte-specific expression. Glia *56*, 481–493.

45. Lee, C.J., Fan, X., Guo, X., and Medin, J.A. (2011). Promoter-specific lentivectors for long-term, cardiac-directed therapy of Fabry disease. J. Cardiol. *57*, 115–122.

46. Zincarelli, C., Soltys, S., Rengo, G., and Rabinowitz, J.E. (2008). Analysis of AAV serotypes 1-9 mediated gene expression and tropism in mice after systemic injection. Mol. Ther. *16*, 1073–1080.

47. Schuster, D.J., Dykstra, J.A., Riedl, M.S., Kitto, K.F., Belur, L.R., McIvor, R.S., Elde, R.P., Fairbanks, C.A., and Vulchanova, L. (2014). Biodistribution of adeno-associated virus serotype 9 (AAV9) vector after intrathecal and intravenous delivery in mouse. Front. Neuroanat. *8*, 42.

48. Philpot, B.D., Men, D., McCarty, R., and Brunjes, P.C. (1998). Activity-dependent regulation of dopamine content in the olfactory bulbs of naris-occluded rats. Neuroscience *85*, 969–977.

49. Cummings, D.M., and Belluscio, L. (2010). Continuous neural plasticity in the olfactory intrabulbar circuitry. J. Neurosci. *30*, 9172–9180.

50. Adamek, G.D., Gesteland, R.C., Mair, R.G., and Oakley, B. (1984). Transduction physiology of olfactory receptor cilia. Brain Res. *310*, 87–97.

51. Mockel, A., Perdomo, Y., Stutzmann, F., Letsch, J., Marion, V., and Dollfus, H. (2011). Retinal dystrophy in Bardet-Biedl syndrome and related syndromic ciliopathies. Prog. Retin. Eye Res. *30*, 258–274.

52. Gerth, C., Zawadzki, R.J., Werner, J.S., and Héon, E. (2008). Retinal morphology in patients with BBS1 and BBS10 related Bardet-Biedl Syndrome evaluated by Fourier-domain optical coherence tomography. Vision Res. *48*, 392–399.

53. Azari, A.A., Aleman, T.S., Cideciyan, A.V., Schwartz, S.B., Windsor, E.A., Sumaroka, A., Cheung, A.Y., Steinberg, J.D., Roman, A.J., Stone, E.M., et al. (2006). Retinal disease expression in Bardet-Biedl syndrome-1 (BBS1) is a spectrum from maculopathy to retina-wide degeneration. Invest. Ophthalmol. Vis. Sci. *47*, 5004–5010.

54. Simons, D.L., Boye, S.L., Hauswirth, W.W., and Wu, S.M. (2011). Gene therapy prevents photoreceptor death and preserves retinal function in a Bardet-Biedl syndrome mouse model. Proc. Natl. Acad. Sci. USA *108*, 6276–6281.

55. Schwob, J.E. (2002). Neural regeneration and the peripheral olfactory system. Anat. Rec. *269*, 33–49.

56. Jooss, K., and Chirmule, N. (2003). Immunity to adenovirus and adeno-associated viral vectors: implications for gene therapy. Gene Ther. *10*, 955–963.

57. Samulski, R.J., Zhu, X., Xiao, X., Brook, J.D., Housman, D.E., Epstein, N., and Hunter, L.A. (1991). Targeted integration of adeno-associated virus (AAV) into human chromosome 19. EMBO J. *10*, 3941–3950.

58. Kotin, R.M., Siniscalco, M., Samulski, R.J., Zhu, X.D., Hunter, L., Laughlin, C.A., McLaughlin, S., Muzyczka, N., Rocchi, M., and Berns, K.I. (1990). Site-specific integration by adeno-associated virus. Proc. Natl. Acad. Sci. USA *87*, 2211–2215.

59. Cheung, A.K., Hoggan, M.D., Hauswirth, W.W., and Berns, K.I. (1980). Integration of the adeno-associated virus genome into cellular DNA in latently infected human Detroit 6 cells. J. Virol. *33*, 739–748.

60. Mackay-Sim, A., and Kittel, P. (1991). Cell dynamics in the adult mouse olfactory epithelium: a quantitative autoradiographic study. J. Neurosci. *11*, 979–984.

61. Hinds, J.W., Hinds, P.L., and McNelly, N.A. (1984). An autoradiographic study of the mouse olfactory epithelium: evidence for long-lived receptors. Anat. Rec. *210*, 375–383.

62. Miragall, F., Krause, D., de Vries, U., and Dermietzel, R. (1994). Expression of the tight junction protein ZO-1 in the olfactory system: presence of ZO-1 on olfactory sensory neurons and glial cells. J. Comp. Neurol. *341*, 433–448.

63. Hussar, P., Tserentsoodol, N., Koyama, H., Yokoo-Sugawara, M., Matsuzaki, T., Takami, S., and Takata, K. (2002). The glucose transporter GLUT1 and the tight junction protein occludin in nasal olfactory mucosa. Chem. Senses *27*, 7–11.

64. Brittebo, E.B. (1995). Metabolism-dependent toxicity of methimazole in the olfactory nasal mucosa. Pharmacol. Toxicol. *76*, 76–79.

65. Bergman, U., and Brittebo, E.B. (1999). Methimazole toxicity in rodents: covalent binding in the olfactory mucosa and detection of glial fibrillary acidic protein in the olfactory bulb. Toxicol. Appl. Pharmacol. *155*, 190–200.

66. Schwob, J.E., Youngentob, S.L., and Mezza, R.C. (1995). Reconstitution of the rat olfactory epithelium after methyl bromide-induced lesion. J. Comp. Neurol. *359*, 15–37.

67. Leung, C.T., Coulombe, P.A., and Reed, R.R. (2007). Contribution of olfactory neural stem cells to tissue maintenance and regeneration. Nat. Neurosci. *10*, 720–726.

68. Gregory, L.G., Harbottle, R.P., Lawrence, L., Knapton, H.J., Themis, M., and Coutelle, C. (2003). Enhancement of adenovirus-mediated gene transfer to the airways by DEAE dextran and sodium caprate in vivo. Mol. Ther. *7*, 19–26.

69. Sakai, M., Imai, T., Ohtake, H., Azuma, H., and Otagiri, M. (1997). Effects of absorption enhancers on the transport of model compounds in Caco-2 cell monolayers: assessment by confocal laser scanning microscopy. J. Pharm. Sci. *86*, 779–785.

70. Castellani, S., Di Gioia, S., Trotta, T., Maffione, A.B., and Conese, M. (2010). Impact of lentiviral vector-mediated transduction on the tightness of a polarized model of airway epithelium and effect of cationic polymer polyethylenimine. J. Biomed. Biotechnol. *2010*, 103976.

71. Cmielewski, P., Anson, D.S., and Parsons, D.W. (2010). Lysophosphatidylcholine as an adjuvant for lentiviral vector mediated gene transfer to airway epithelium: effect of acyl chain length. Respir. Res. *11*, 84.

72. Stocker, A.G., Kremer, K.L., Koldej, R., Miller, D.S., Anson, D.S., and Parsons, D.W. (2009). Single-dose lentiviral gene transfer for lifetime airway gene expression. J. Gene Med. *11*, 861–867.

73. Zaghloul, N.A., Liu, Y., Gerdes, J.M., Gascue, C., Oh, E.C., Leitch, C.C., Bromberg, Y., Binkley, J., Leibel, R.L., Sidow, A., et al. (2010). Functional analyses of variants reveal a significant role for dominant negative and common alleles in oligogenic Bardet-Biedl syndrome. Proc. Natl. Acad. Sci. USA *107*, 10602–10607.

74. Wei, Q., Zhang, Y., Li, Y., Zhang, Q., Ling, K., and Hu, J. (2012). The BBSome controls IFT assembly and turnaround in cilia. Nat. Cell Biol. *14*, 950–957.

75. Pan, X., Ou, G., Civelekoglu-Scholey, G., Blacque, O.E., Endres, N.F., Tao, L., Mogilner, A., Leroux, M.R., Vale, R.D., and Scholey, J.M. (2006). Mechanism of transport of IFT particles in C. elegans cilia by the concerted action of kinesin-II and OSM-3 motors. J. Cell Biol. *174*, 1035–1045.

76. Ou, G., Koga, M., Blacque, O.E., Murayama, T., Ohshima, Y., Schafer, J.C., Li, C., Yoder, B.K., Leroux, M.R., and Scholey, J.M. (2007). Sensory ciliogenesis in Caenorhabditis elegans: assignment of IFT components into distinct modules based on transport and phenotypic profiles. Mol. Biol. Cell *18*, 1554–1569.

77. Datta, P., Allamargot, C., Hudson, J.S., Andersen, E.K., Bhattarai, S., Drack, A.V., Sheffield, V.C., and Seo, S. (2015). Accumulation of non-outer segment proteins in the outer segment underlies photoreceptor degeneration in Bardet-Biedl syndrome. Proc. Natl. Acad. Sci. USA *112*, E4400–E4409.

78. Xu, Q., Zhang, Y., Wei, Q., Huang, Y., Li, Y., Ling, K., and Hu, J. (2015). BBS4 and BBS5 show functional redundancy in the BBSome to regulate the degradative sorting of ciliary sensory receptors. Sci. Rep. *5*, 11855.

79. Zhang, Q., Seo, S., Bugge, K., Stone, E.M., and Sheffield, V.C. (2012). BBS proteins interact genetically with the IFT pathway to influence SHH-related phenotypes. Hum. Mol. Genet. *21*, 1945–1953.

80. Zolotukhin, S., Byrne, B.J., Mason, E., Zolotukhin, I., Potter, M., Chesnut, K., Summerford, C., Samulski, R.J., and Muzyczka, N. (1999). Recombinant adeno-associated virus purification using novel methods improves infectious titer and yield. Gene Ther. *6*, 973–985.

YMTHE, Volume *25*

Supplemental Information

Gene Therapeutic Reversal of Peripheral Olfactory Impairment in Bardet-Biedl Syndrome

Corey L. Williams, Cedric R. Uytingco, Warren W. Green, Jeremy C. McIntyre, Kirill Ukhanov, Arthur D. Zimmerman, Dana T. Shively, Lian Zhang, Darryl Y. Nishimura, Val C. Sheffield, and Jeffrey R. Martens

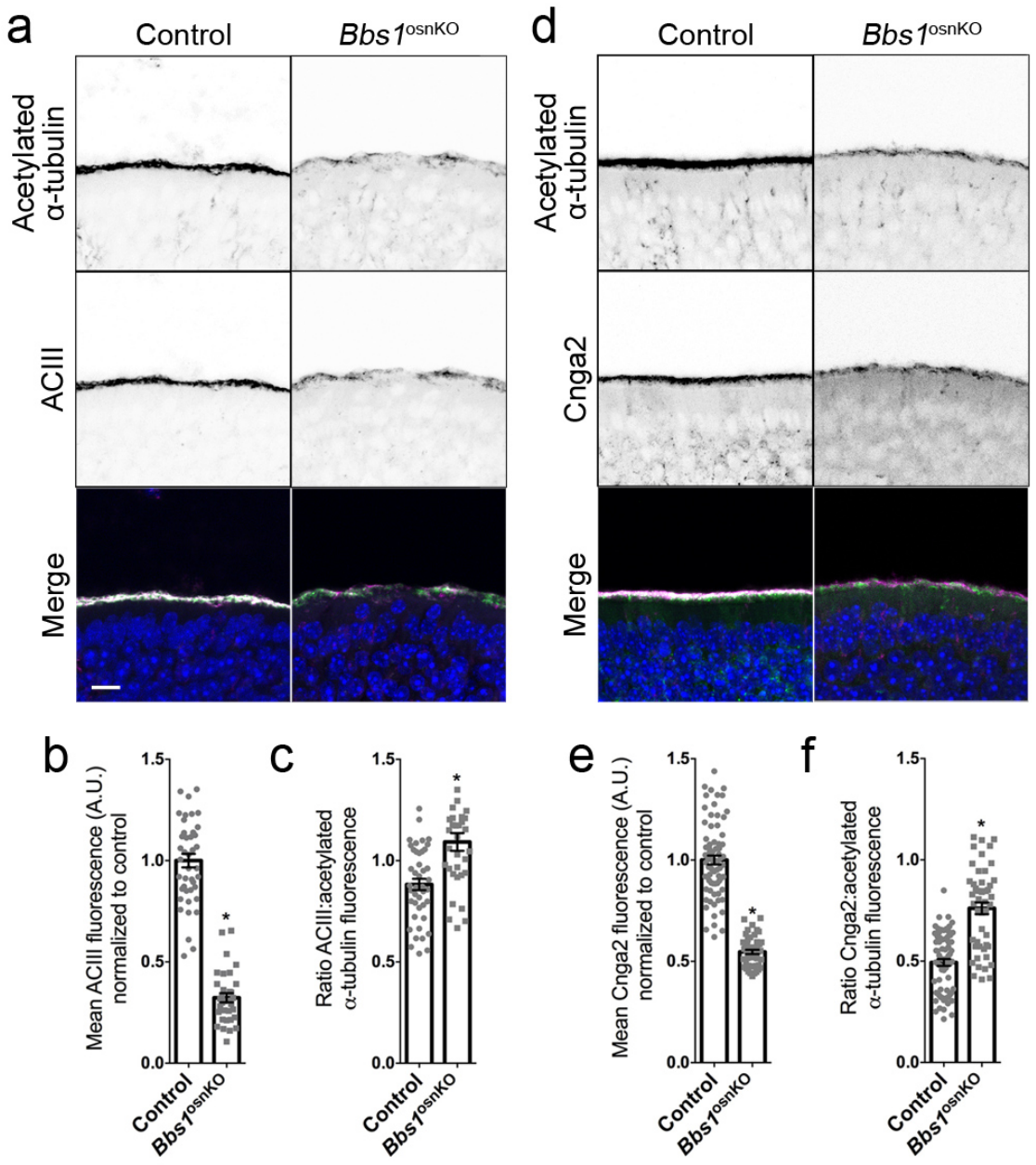
a
Control
Bbs1osnKO
Acetylated α-tubulin
ACIII
Merge
d
Control
Bbs1osnKO
Acetylated α-tubulin
Cnga2
Merge
b
Mean ACIII fluorescence (A.U.) normalized to control
1.5
1.0
0.5
0.0
*
Control
Bbs1osnKO
c
Ratio ACIII:acetylated α-tubulin fluorescence
1.5
1.0
0.5
0.0
*
Control
Bbs1osnKO
e
Mean Cnga2 fluorescence (A.U.) normalized to control
1.5
1.0
0.5
0.0
*
Control
Bbs1osnKO
f
Ratio Cnga2:acetylated α-tubulin fluorescence
1.5
1.0
0.5
0.0
*
Control
Bbs1osnKO

Fig. S1. Apical enrichment of ACIII and Cnga2 is retained in the OE of *Bbs1*^{osnKO} mutants. (*a*) Representative confocal images of coronal sections through olfactory epithelium of control and mutant mice, immunostained for (*top*) acetylated α-tubulin to reveal ciliary microtubules and (*middle*) adenylate cyclase 3 (ACIII). Compared (*left*) control, (*right*) *Bbs1*^{osnKO} tissue has diminished ACIII in the cilia layer on the apical surface of the OE. *(b*) Quantified data showing a significant reduction of ACIII fluorescence intensity in mutants versus controls. Student's t-test, * $p<0.0001$. (*c*) Quantified data showing changes to the ratio of ACIII to acetylated α-tubulin signal intensity at the apical OE surface in mutants versus controls. Student's t-test, * $p<0.0001$. (*d*) Representative confocal images of coronal sections through olfactory epithelium of control and mutant mice, immunostained for (*top*) acetylated α-tubulin and (*middle*) cyclic nucleotide-gated channel alpha 2 (Cnga2). Compared (*left*) control, (*right*) *Bbs1*^{osnKO} tissue has diminished Cnga2 in the cilia layer on the apical surface of the OE. *(e*) Quantified data showing a significant reduction of Cnga2 fluorescence intensity in mutants versus controls. Student's t-test, * $p<0.0001$. (*f*) Quantified data showing changes to the ratio of Cnga2 to acetylated α-tubulin signal intensity at the apical OE surface in mutants versus controls. Student's t-test, * $p<0.0001$. Values represent means ± SEM. Scale bar, 10 μm.

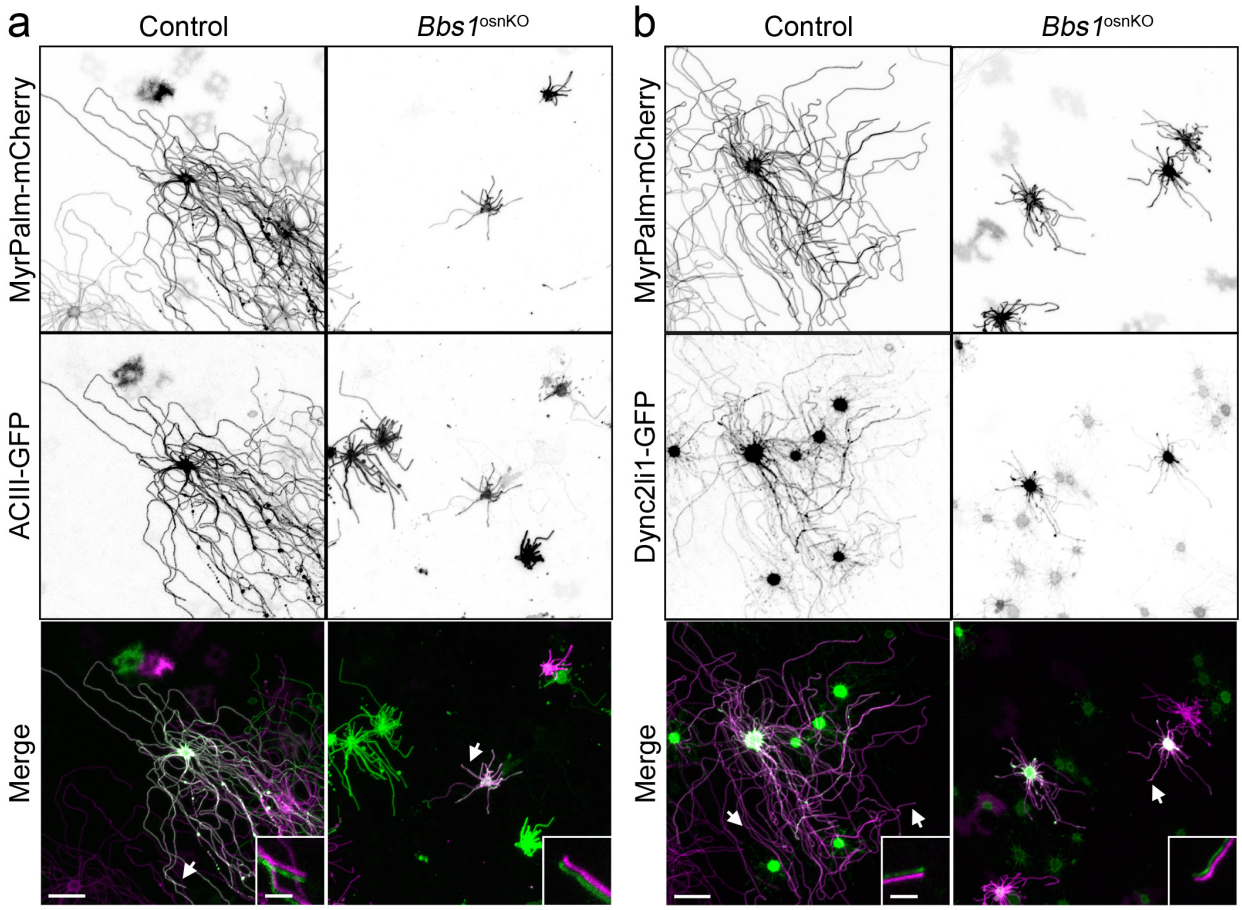

Fig. S2. OSN ciliation is diminished in *Bbs1*^{osnKO} mutants, but ACIII and Dync2li1 localization is unaffected. (*a*) Representative live *en face* images of ectopic (*top*) MyrPalm-mCherry and (*middle*) ACIII-GFP expression in olfactory epithelium of (*left*) control and (*right*) *Bbs1*^{osnKO} mice. Insets show magnified and color-shifted ciliary tips, corresponding to arrows. Compared to control, ciliary membrane distribution of ACIII-GFP and MyrPalm-mCherry appears normal in residual cilia of *Bbs1*^{osnKO} OSNs. (*b*) Representative live *en face* images of ectopic (*top*) MyrPalm-mCherry and (*middle*) GFP-tagged cytoplasmic dynein 2 light intermediate chain 1 (Dync2li1-GFP) expression in olfactory epithelium of (*left*) control and (*right*) *Bbs1*^{osnKO} mice. Insets show magnified and color-shifted ciliary tips, corresponding to arrows. Similar to control, Dync2li1-GFP is capable of localizing to tips of *Bbs1*^{osnKO} OSN cilia. Scale bars, 10 μm; 1.25 μm (insets).

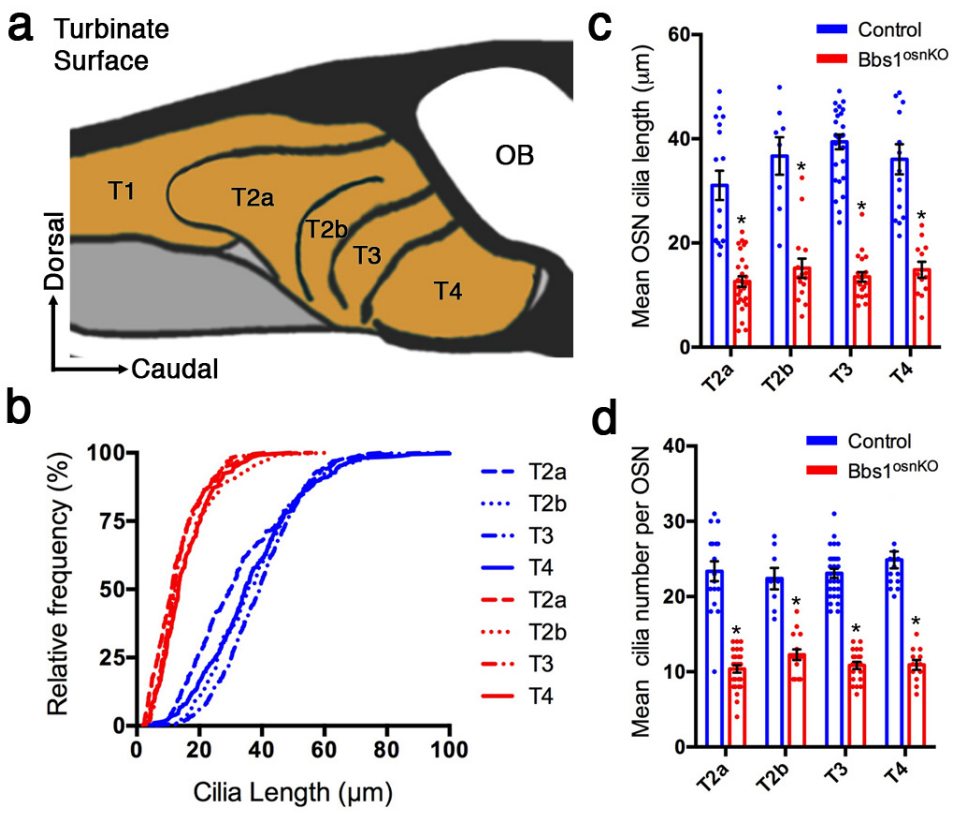

Fig. S3. Uniform olfactory cilia loss across the turbinates OE of *Bbs1*^{osnKO} mutant mice. (*a*) Diagram depicting the regional organization of (*orange*) turbinate olfactory epithelium (TOE) relative to the nasal cavity and olfactory bulb (OB). (*b*) Cumulative distribution of cilia lengths from (*blue*) control and (*red*) *Bbs1*^{osnKO} animals *en face* confocal images from different turbinate regions (control n=1595 cilia on 68 OSNs; *Bbs1*^{osnKO} n=812 cilia on 74 OSNs). (*c*) Quantification of reduced OSN cilia length in (*red*) *Bbs1*^{osnKO} mutants compared to (*blue*) controls, measured from live *en face* confocal images of AV5-mediated ectopically expressed MyrPalm-mCherry in different turbinate regions. Two-Way ANOVA. $F_{(1,134)}$=236.0, *p<0.0001. Post-hoc Bonferroni test. (*d*) Quantification of reduced OSN cilia number in *Bbs1*^{osnKO} mutants. Two-Way ANOVA. $F_{(1,134)}$=396.3, *p<0.0001. Post-hoc Bonferroni test. Values represent means ± SEM.

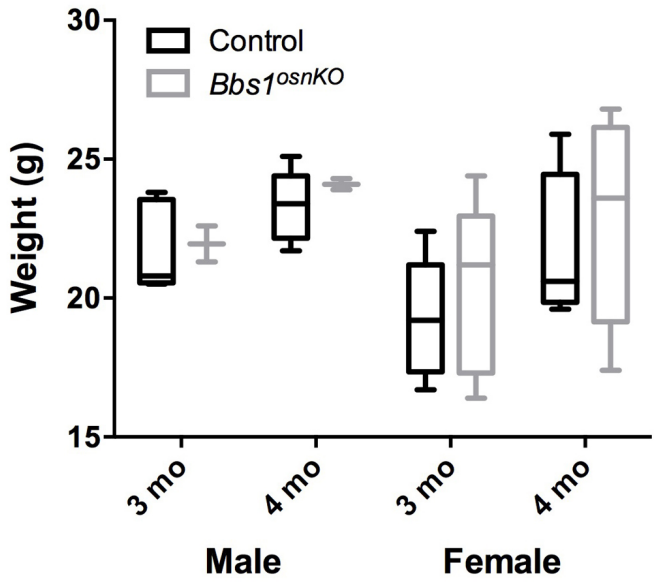

Fig. S4. Olfactory-specific disruption of BBS1 does not induce obesity. *Bbs1*^{osnKO} animals and control littermates were fed *ad libitum* and weighed at three and four months of age. There were no significant differences (Student's t-test, $p>0.05$) between the weights of control and *Bbs1*^{osnKO} mutant (*left*) males or (*right*) females. n=5 control males, 2 *Bbs1*^{osnKO} males, 5 control females, 5 *Bbs1*^{osnKO} females. Values represent means ± SD and min/max.

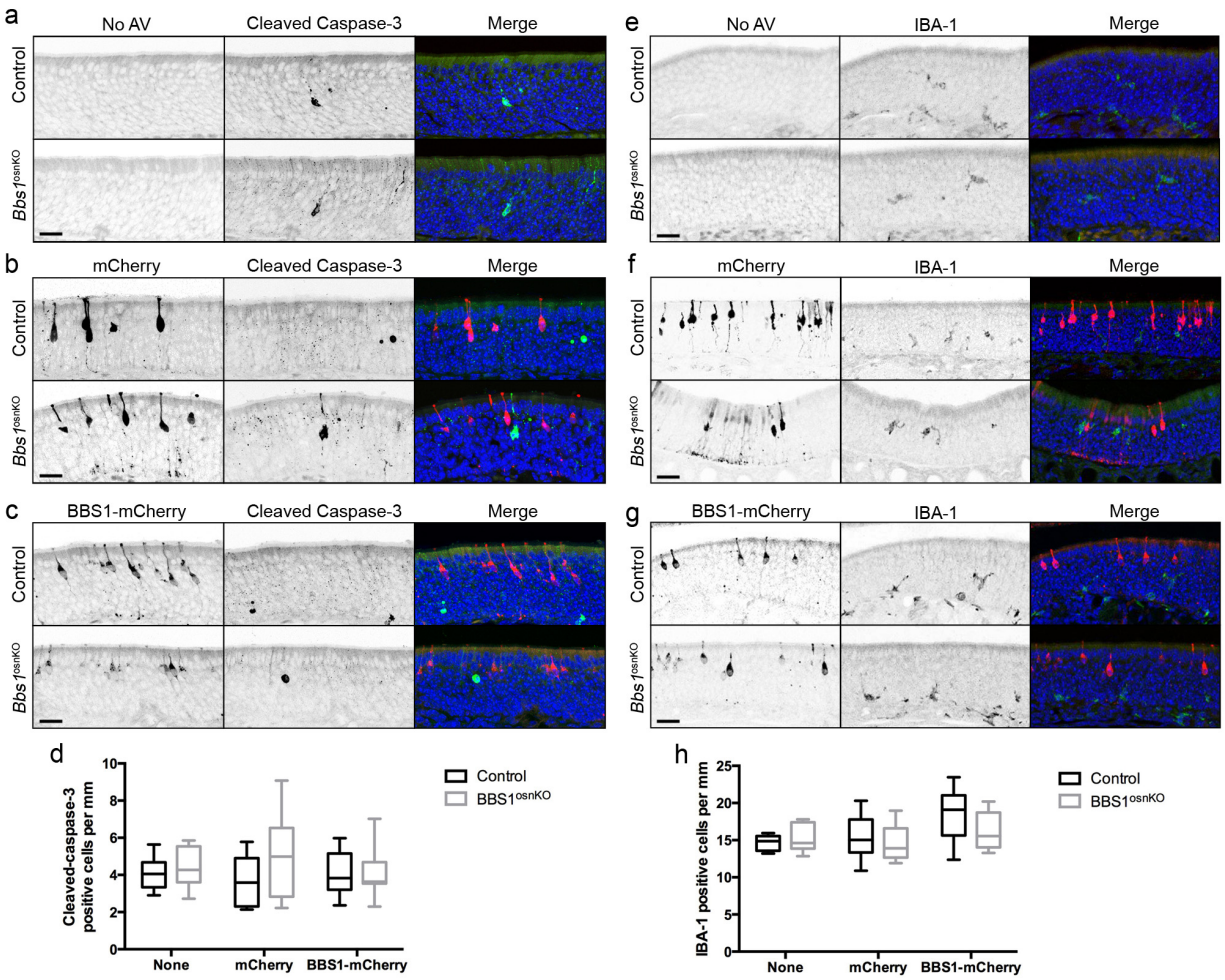
a
No AV
Cleaved Caspase-3
Merge
Control
Bbs1osnKO
b
mCherry
Cleaved Caspase-3
Merge
c
BBS1-mCherry
Cleaved Caspase-3
Merge
e
No AV
IBA-1
Merge
f
mCherry
IBA-1
Merge
g
BBS1-mCherry
IBA-1
Merge
d
Cleaved-caspase-3 positive cells per mm
None
mCherry
BBS1-mCherry
Control
BBS1osnKO
h
IBA-1 positive cells per mm
None
mCherry
BBS1-mCherry
Control
BBS1osnKO

Fig. S5. BBS1 overexpression does not induce apoptosis and macrophage infiltration in the OE. (*a-c*) Representative confocal images of cleaved caspase-3 immunostaining in fixed coronal sections of control and *Bbs1*^{osnKO} mutant OE following (*a*) no treatment, or AV-mediated expression of (*b*) mCherry or (*c*) BBS1-mCherry. (*d*) Quantification of cleaved caspase-3 immunostaining in the OE of untreated control or *Bbs1* osnKO mutants and animals treated with AV-mCherry or AV-BBS1-mCherry. n=3 animals per condition. Student's t-test showed no statistical difference between any groups. (*e-g*) Representative confocal images of IBA-1 immunostaining in fixed coronal sections of control and *Bbs1*^{osnKO} mutant OE following (*e*) no treatment, or AV-mediated expression of (*f*) mCherry or (*g*) BBS1-mCherry. (*h*) Quantification of cleaved caspase-3 immunostaining in the OE of untreated control or *Bbs1* osnKO mutants and animals treated with AV-mCherry or AV-BBS1-mCherry. n=3 animals per condition. Student's t-test showed no statistical difference between any groups. Values represent means ± SD and min/max. Scale bar, 20 μm (*a-c, e-g*).

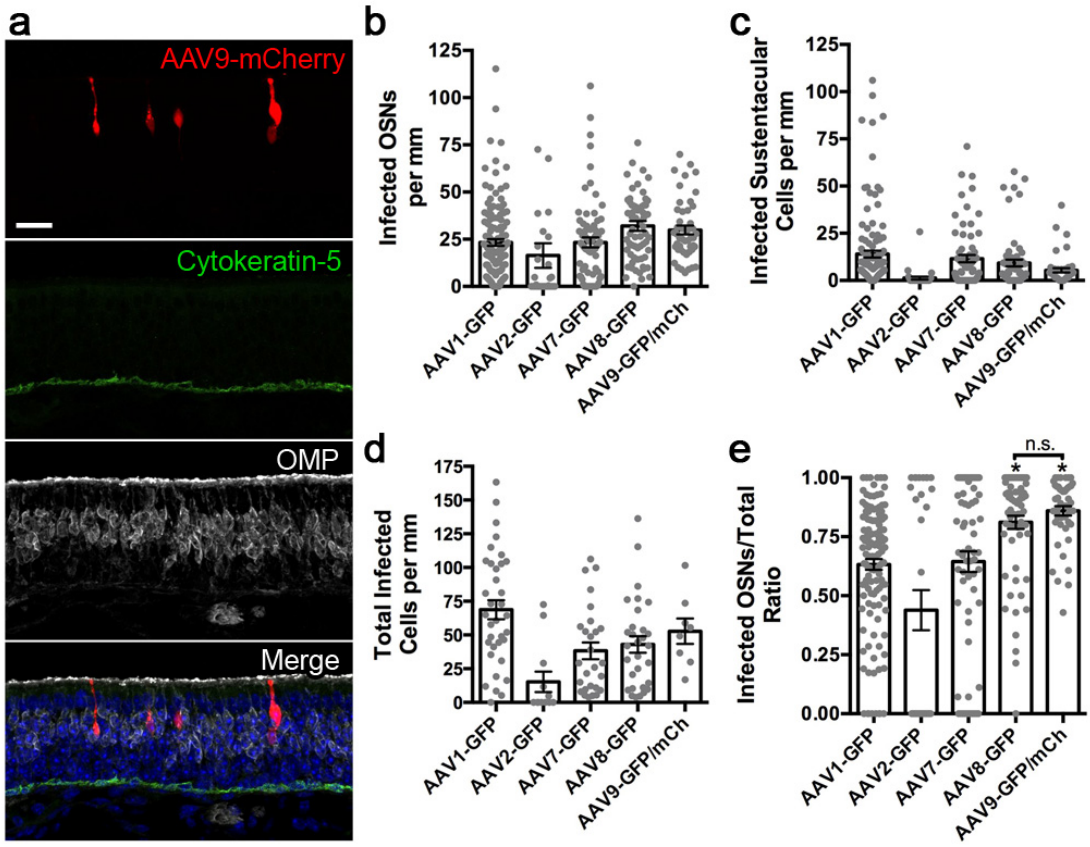

Fig. S6. Adeno-associated viral infection specificity in OE. (*a*) Representative image shows a fixed coronal section of OE from control mice 3 weeks after treatment with AAV9-mCherry. Coronal section was immunostained for cytokeratin-5 to reveal horizontal basal cells and olfactory marker protein (OMP) to reveal mature OSNs. (*b-e*) Quantification of AAV infected (*b*) OSNs, (*c*) sustentacular cells, and (*d*) total cells per mm of OE. (*e*) Quantified data showing changes to the ratio of infected OSNs cells relative to total infected cells on OE surface of control animals across different AAV serotypes. Compared to other AAV serotypes, AAV8 and AAV9-mediated expression show significantly higher relative OSN infection. n = 3 animals per condition. One-way ANOVA, $F_{(4,334)}=14.03$, *p<0.0001, Tukey Post-hoc. Values represent means ± SEM. Scale bar, 20 μm (*a*).